Tide-influenced deltas: The ebb and flow of a system at work

A THESIS
SUBMITTED TO THE FACULTY OF
UNIVERSITY OF MINNESOTA
BY

Nathan Lentsch

IN PARTIAL FULFILLMENT OF THE REQUIREMENTS
FOR THE DEGREE OF
MASTER OF SCIENCE

Dr. Chris Paola, Advisor

August 2017

Acknowledgements

The fact that I am here reflecting on our research and this thesis is testament to the many people who have helped me along the way.

First and foremost, I have to thank John Swenson for setting me down this sediment-laden path. The innumerable conversations we had, your enthusiasm in my academic journey and your sincere desire to see me succeed had more of an impact on me than I can ever convey to you. Thank you for everything.

My undergraduate advisor Vicki Hansen was instrumental in getting me to this point, but more than academic advice, her genuine care for both my wife and me has touched us both. We will both always consider you a friend of the family.

To my advisor Chris Paola, I am indebted to you for taking on a salty veteran two years ago. While you were always there to guide me and answer my questions, I truly appreciated how much you let me navigate these experiments on my own. I hope the work I showcase here in this thesis lives up to the high standards that SAFL is known for. Lastly, your interest in my academic and professional career will leave me forever grateful. This next leg of my journey is thanks, in no small part, to you.

To my other committee members, Crystal and Andy, thank you so much for your valuable input. It was greatly appreciated and really made a difference to the clarity of this work.

The engineering staff at SAFL is second to none and I have to specifically thank Chris Ellis, Dick Christopher, Erik Steen and Ben Erickson for their tireless support of our research. You are the unsung heroes of SAFL and no project would be possible without you and your staff.

A big thank you to my peers in the Sediment Transport Group at SAFL, especially for answering all of this newbie's questions and aiding me with different types of analysis. You all helped lay the foundation for this work.

Lastly, to my partner in crime Alvise Finotello, thanks for dragging me along on your crazy tidal adventure. None of the work here would be possible without your tireless effort. You are much more than just a collaborator; you have become a true friend. I look forward to another couple of decades of Aperol filled nights.

Dedication

Road to a Thesis

This thesis is the culmination of a very untraditional academic career:

- 2003 – Graduated high school
- 2005 – Joined the Air Force after avulsing out of college
- 2005 – Prograded to become an Explosive Ordnance Disposal Technician
- 2006 – Stationed in Germany and deployed to Iraq
- 2007 – 4,367 miles from home, met my German soulmate
- 2008 – A sad bifurcation sees me relocated to South Korea
- 2009 – Meandered to Japan and deployed to Kyrgyzstan and Afghanistan
- 2010 – After over two years apart, we finally reached the matrimony confluence
- 2011 – Separated active duty and started at UMD eight years delayed
- 2013 – Discovered my love of sedimentology
- 2014 – Life was put on hold again, deployed to aeolian-driven Kuwait
- 2015 – Graduated UMD and began an 8,430 tidal cycle adventure
- 2017 – Finally reached the delta at the end of my academic river
- 2017 – As one chapter closes another begins; the first Lentsch tributary is born

Getting to this milestone in my life is thanks to my parents. Thank you for never giving up on the hell raiser that clearly needed military and German wife intervention.

To my amazing wife Hanna, I do not even know where to begin. Your unwavering support through my academic, military and professional careers is the only reason I was successful at any of them. You truly are the bedrock of this family and I will always consider myself the luckiest man to have found you. I can never repay you for uprooting your life for me and my goals, and I only hope you let me repay some of that debt by being the best husband I can be. I am truly blessed to have you as wife and the mother of our children. As we meander down this new river called parenthood, there is no one else I would want as my shipmate.

Table of Contents

List of Tables

List of Figures

1

Introduction

Rivers are dynamic conduits through which drainage basins evacuate accumulated surface water from rain or melting snow and ice. The erosive properties of flowing water over bedrock and loose sediment turn rivers into sediment super highways, with the larger North American rivers alone having suspended sediment loads of 10^4-10^7 metric tons a year (Heimann et al., 2011). Ultimately, most of the world's rivers meet a relatively stagnant body of water at their terminus, which causes current deceleration within the channels. For rivers joining the ocean, this loss of energy by the river channel causes vast amounts of sediment to be deposited at the coast. Where the rate of this sediment deposition outpaces local subsidence, we see the birth of a delta.

Deltas are some of the largest depositional features on Earth and while they are built by sediment, they are much more than just gravel, sand and mud. The very same rivers that build deltas also carry with them fluxes of nutrients that make deltas ideal for agriculture and aquaculture. As such, even though deltas account for less than 1% of global land area, they are densely populated with plants, animals and humans, the latter population now over 500 million (Ericson et al., 2006). Rivers, however, are not the only morphodynamic drivers that shape the delta landscape these populations depend on.

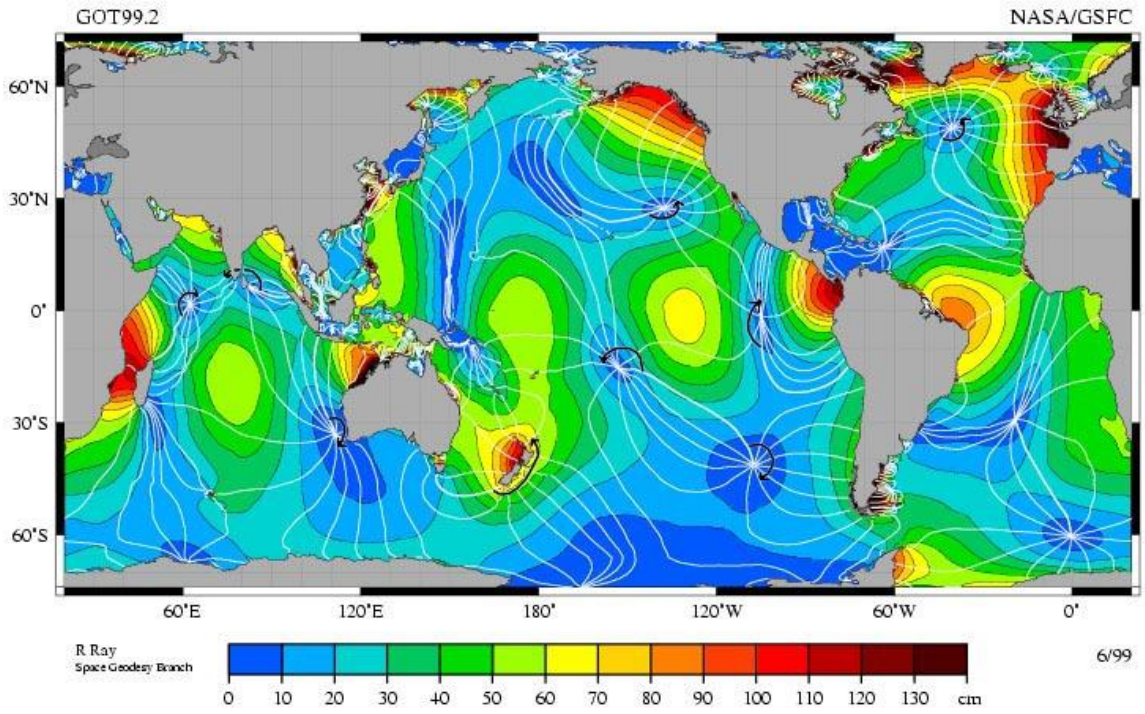

Figure 1.1: The lunar, or M2, tidal constituent with amplitude indicated by color. White lines are cotidal lines which indicate simultaneous tide levels (R. Ray, TOPEX/Poseidon: Revealing Hidden Tidal Energy, GSFC, NASA).

Being sited on the world's coasts exposes deltas to a host of marine processes which can affect the morphodynamics and net deposition of the subaerial and subaqueous delta components. Of these allogenic forces, tides are one of the most prevalent and their effect on delta morphology led to their inclusion in classifying delta types (Galloway, 1975). In fact, all the coastlines of the world are influenced by tides (Figure 1.1), with some coastlines seeing daily tidal amplitudes over 5 m (Bernier and Thompson, 2010). Where river outlets and these large tidal amplitudes overlap, we see the formation of tide-dominated deltas (Figure 1.2).

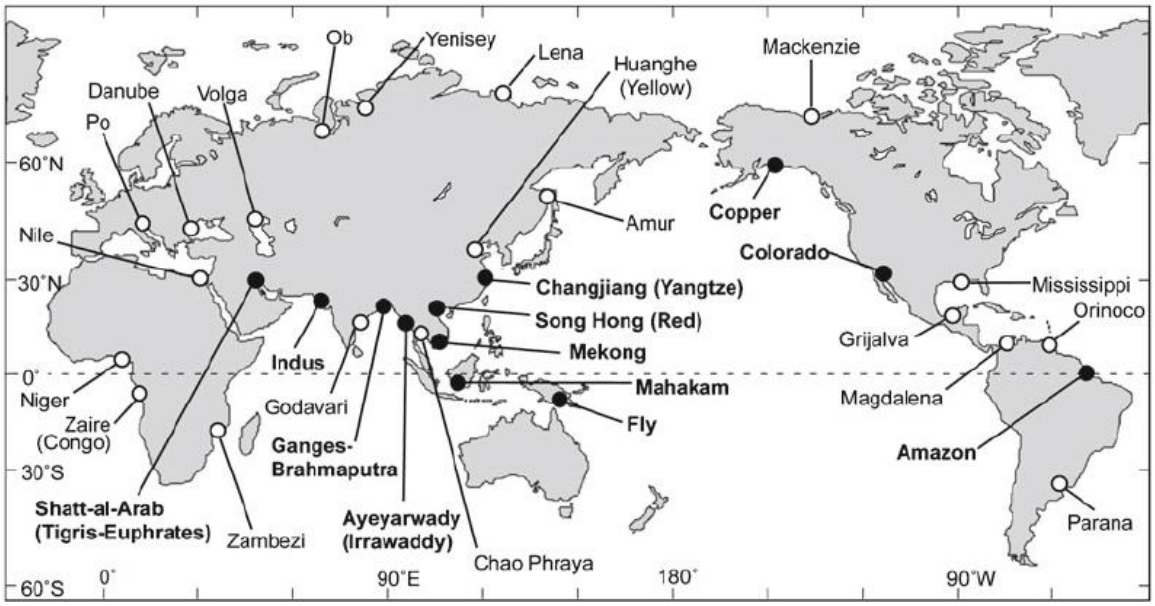

Figure 1.2: Map of the world's major river delta systems, with those forming tide-dominated deltas indicated by bold type and filled circles. From Goodbred and Saito (2012), modified after Hori and Saito (2007).

As seen in Figure 1.2, major tide-dominated deltas are distributed across the globe and their average subaerial landmass ranks them as some of the largest deltas in the world (Woodroffe et al., 2006). Yet for all their size, tide-influenced deltas are typically only a few meters above sea level at their extent; the largest tidal delta in the world, the Ganges-Brahmaputra, is only 5 m above sea level (Akter et al., 2016). With typical slopes of $1 \cdot 10^{-5}$ (Wilson and Goodbred, 2015), tide-influenced deltas are vulnerable to both local and eustatic sea-level rise, with the latter phenomenon projected to increase global mean sea level by at least 0.5 m in the next century (Church et al., 2013). While understanding delta response to relative sea-level (RSL) rise is a critical scientific question for all deltas, it is especially crucial for tide-influenced deltas as high tide may increase the reach of eustatic rise.

In this thesis, we present a suite of experiments conducted in Saint Anthony Falls

Laboratory's delta basin facilities. These experiments explore how tide-influenced deltas respond to RSL rise, as well as how this response compares to that of river deltas with no tidal forcing. Presented as separate journal articles, the following chapters focus on different aspects of tide-influenced deltas and further our understanding of these complex systems.

In Chapter 2, we present 10 physical experiments that vary in their fluvial to tidal energies, rates of RSL rise and sediment budgets. Using traditional data collection methods (e.g., high resolution topographic scans), we introduce new methods of analysis to study net deposition and the morphologic response of experimental deltas. These experiments also generate further questions of tidal influence on river deltas based on qualitative observations of channel dynamics. Therefore, Chapter 3 explores the apparent reduction in distributary channel mobility in deltas affected by tides and presents novel techniques for quantifying channel mobility from both time-lapse photography and digital elevation model data. Finally, Chapter 4 concludes this thesis with a summary of results and a look forward into the experiments of tomorrow.

2

Experimental delta evolution in tidal environments: Morphologic response to sea-level rise and net deposition*

*****To be submitted as Lentsch, N., Finotello, A., and Paola, C. *Experimental delta evolution in tidal environments: Morphologic response to sea-level rise and net deposition* to Journal of Geophysical Research: Earth Surface.

SYNOPSIS

Tide-influenced deltas are among the largest depositional features on Earth and are ecologically and economically important. However, the continued rise in relative sea level threatens the sustainability of these landscapes and calls for new insights on their morphological response. While field studies of ancient deposits allow for insight into delta evolution during times of eustatic adjustment, tidal deltas are notoriously hard to identify in the rock record. Here we present a suite of physical experiments aimed at reproducing tide-influenced deltas subjected to relative sea-level (RSL) rise. Using new analysis techniques, we employ topographic profiles to classify upstream and downstream net deposition as well as shoreline migration across the delta topset. These profiles are further used in a new method for comparing transgression rates across systems with varying sediment budgets. By altering the ratio of fluvial to tidal energy, we show that tide-influenced deltas are subjected to shoreline transgression as compared to identical, yet purely fluvial, deltas that exhibit static or even regressive shorelines. Different magnitudes of net deposition among our experiments clearly reveal how tides

effectively remove sediment, which would otherwise be deposited by fluvial processes, from the delta topset. Furthermore, strong tidal forcing can reduce the mobility of distributary channels and create composite deltas were different processes dominate varying areas of the delta plain leading to distinct morphologies.

1. INTRODUCTION

River deltas are landforms that form from sediment delivered by rivers to coastal areas by means of interconnected channel pathways (Tejedor et al., 2015). Deltas evolving under the influence of tides are of particular importance as most of the largest modern rivers feed either tide-dominated or tide-influenced deltas (Tänavsuu-Milkeviciene and Plink-Björklund, 2009) and their associated subaerial and subaqueous landmasses make them some of the largest sedimentary environments on Earth (Woodroffe et al., 2006). Moreover, the fecund, wide plains created by the combined action of fluvial and tidal processes attract large human populations (Goodbred and Saito, 2012), providing an invaluable asset for some of the largest economies worldwide. Example systems include the tide-dominated Changjiang Delta of the Yangtze River which hosts many of the world's largest cities -- Shanghai alone has a population density of 2,145 inhabitants per square kilometer (Tian et al., 2011) -- as well as the tide-dominated Ganges-Brahmaputra Delta which hosts nearly 2% of the world's population even though half of its area is within 5 m of mean sea level (Akter et al., 2016). However, the steady rise in RSL currently experienced by most tide-influenced deltas threatens the stability of these landscapes and consequently endangers their populations. Yet little research exists on the response of deltas subjected to tidal processes and eustatic rise.

This may be partially due to the limited number of tidal deltas identified in the rock record (Plink-Björklund, 2012), as several "characteristic" tidal features (e.g., funnel shaped tidal channels, tidal mouth bars, etc.) are not well preserved in the rock record (Dalrymple and Choi, 2007). Physical experiments can help bridge this knowledge gap (Malverti et al., 2008; Paola et al., 2009; Kleinhans et al., 2012; Kleinhans et al., 2014).

Physical models allow for capturing delta evolution at a spatial and temporal resolution that is impractical in the field. Recent studies employing physical experiments have been able to reproduce several typical tidal features, such as ebb deltas (Kleinhans et al., 2012), tidal channel networks (Tambroni et al., 2005; Stefanon et al., 2010; Vlaswinkel and Cantelli, 2011) and tidal estuaries (Kleinhans et al., 2014). However, all of these experiments functioned by allowing tides to rework a layer of hand-laid sediment; due to the limitations of the physical setup or the goals of the research, no sediment was introduced via a fluvial system. As most of the largest modern rivers (in terms of sedimentation) have their mouths along tide-dominated coasts (Middleton, 1991), investigating the autogenic processes occurring in a deltaic system influenced by the action of tides is a logical evolution of coastal research.

Using the delta basin facilities of Saint Anthony Falls Laboratory (SAFL), we conducted a suite of 10 experiments with varying tidal and fluvial energies. These experiments are further characterized by varying sediment discharge and RSL rise rates. In this way, we capture not only the differences in how tidal and non-tidal deltas respond to RSL rise, but also how a delta system adapts morphologically as forcing becomes more dynamic (i.e., high sediment discharge and high RSL rise). In the field, dynamic

tidal coasts have been studied and evolutionary classification schemes have attempted to couple sequence stratigraphy with RSL rise (Boyd et al., 1992). However, these coasts are exposed to multiple marine processes, such as waves and longshore currents, which can have a strong influence on net deposition. A further benefit of conducting tidal delta research in a closed basin lies in the ability to minimize these marine processes and isolate tidal effects.

For these experiments, primary data collection consisted of digital elevation models (DEM), which enabled tracking both shoreline position and net deposition across the delta topset. We present new methods developed to measure the difference between anticipated and actual shoreline migration as well as a new technique for representing the evolution of a delta plain in terms of net deposition. Our results show that (1) all other conditions being equal, tide-dominated deltas transgress as fluvial-dominated deltas remain static or regress under RSL rise. We therefore suggest that (2) tides are effective at removing sediment that would otherwise be deposited on the delta topset. Lastly, (3) in experiments with the strongest tidal forcing, we observed distributary channels that were pinned in place and allowed for the formation of a composite delta as different processes dominated across the delta.

2. EXPERIMENTAL METHODS

2.1 Delta Basin-2 setup

Experiments were conducted in SAFL's Delta Basin-2 (DB-2) facility as this basin can produce deltaic deposits subjected to tidal forcing (Figure 2.1a). This square basin is 5 m by 5 m and has a depth of 0.5 m. Well-mixed sediment and water, whose

quantities were independently and remotely controlled, were fed from a corner of the basin to create a semicircular delta. The feed point source was located behind a gravel diffuser that helped distribute sediment and water evenly and minimized local scour. The base level within the basin was computer controlled through a motorized weir connected to a sonar sensor taking water level measurements every 5 seconds. To produce tides, the basin was connected to a 2 m by 2m, 0.5 m deep auxiliary basin by two industrial pumps. During the flood phase of the tidal cycle, water was pumped into the main basin from the auxiliary basin by the flood pump. After the specified upper tidal limit was reached, the flood pump ceased allowing for slack water on the delta. The ebb pump then brought the water level down to the lower tidal limit and again allowed for a momentary slack water. The tidal amplitude, or half the tidal range, and the tidal period were both computer controlled. The tidal cycle for these experiments was sinusoidal and any deviations from the specified water elevation were identified by the sonar measured water depth. Small changes in voltage to the pumps and the weir allowed for error of less than 1 mm in water elevation.

It is important to note that one limitation of this setup is the inability to effectively create mixed tidal ranges. In nature, several tide-influenced systems experience mixed semidiurnal tide cycles, i.e. they have two high tides and two low tides of different magnitude. Given that we were not attempting to create a detailed scale model of a specific delta but rather to explore overall morphologic effects of tidal pumping, we do not consider this an important limitation.

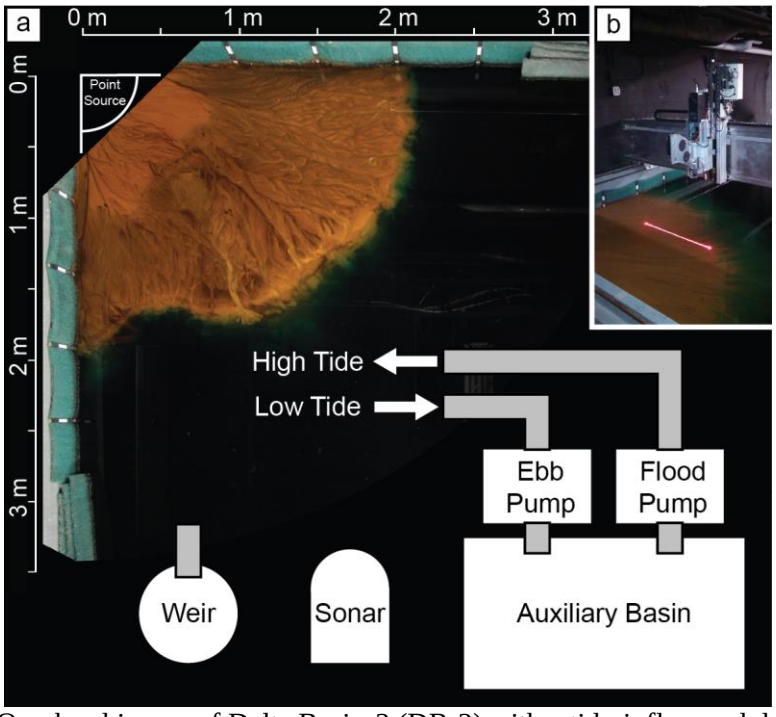

Figure 2.1: (a) Overhead image of Delta Basin-2 (DB-2) with a tide-influenced delta. The added equipment schematics are not drawn to scale. (b) An image of the data cart that serves DB-2. The cart consists of a high-resolution digital line scan camera capable of generating digital elevation models (DEM) with submillimeter resolution. Several overlapping passes were made over the deposit with the final DEM generated from stitching the passes together.

2.2 Methods of data collection

Primary data collection in these experiments consisted of overhead time-lapse photography and periodic digital elevation model (DEM) scans. The photography entailed a digital single-lens reflex camera affixed above the basin with a wide-angle lens to capture the entirety of the deposits. The camera's resolution and height above the basin were such that each pixel is approximately 1 mm by 1 mm in Cartesian space. As a wide angle lens was used, the outer portions of the images were subjected to barrel distortion. Every image was therefore orthorectified in a batch process so that all portions of the deposit were correctly scaled. The camera itself was computer controlled, with the time-lapse between photos specified by the user. All experiments with tides had a time-lapse

interval of half the period to capture both the flood and ebb phase of the tidal cycle. The water used as fluvial discharge was dyed blue at the point source with an industrial food colorant to aid in channel identification within the images. This highly concentrated dye is introduced as a drop every few seconds and therefore has no significant effect on net fluvial discharge.

Additionally, DB-2 is served by a data cart equipped with a high-resolution line scan camera for DEM collection (Figure 2.1b). This camera has a plan view resolution of 1 mm by 1 mm and a vertical resolution of less than 1 mm. Periodically, the experiments were paused and the surface of the deposits were allowed to drain slowly so as to not affect the surface morphology. The data cart took several overlapping scans and once finished, stitched the scans together into one continuous DEM. Water level was then slowly raised to the pre-pause position and the experiment continued until the next scan time.

2.3 Experiment run parameters and initial tidal network

Looking at the effectiveness of physical experiments for reproducing stratigraphy and geomorphologies similar to those seen in the field, Paola et al. (2009) showed that short term base-level cycles on physical models has further refined sequence stratigraphy as a tool. In fact, many of the elements identified in sequence evolution have been reproduced experimentally through base-level cycles meant to represent gradual transgressions or regressions (Ethridge et al., 2009). Here we produced tidal environments experimentally by creating base-level cycles with a much shorter period (2 min) and a set tidal range (20 or 7 mm from high to low tide). This frequency of base-

level variation created channels with bidirectional flow perpendicular to the shoreline that was strong enough to mobilize sediment during the flood and ebb phases of the tide. The period used in these experiments was the same used by Baumgardner (2015) as she points out that this time scale is shorter than the avulsion timescale but long enough to allow for a quasi-steady current in the tidal channels.

A total of 10 experiments were conducted imposing different water and sediment discharges, tidal amplitudes and periods, and sea-level rise rates (Table 2.1). Tidal amplitudes were selected based on their corresponding energies; 10 mm amplitude tides had energies greater than the associated fluvial system, while 3.5 mm amplitude tides had lower energies, making it possible to specify the system as tide-dominated or tide-influenced. These energies are reported in power per unit length in the streamwise direction and their formulas have been used to classify both deltas in the field and in physical experiments (Baumgardner, 2015).

Table 2.1 Experiment Parameters and Energies

Experiment	Sea-level Rise [mm/hr]	Water Discharge [m^3/s]	Sediment Discharge [m^3/s]	Tide Amplitude [mm]	Tide Period [sec]	Tidal Power [W/m][a]	Fluvial Power [W/m][a]
DB2-1600	0.5	0	0	10.0	120	4.09e-2	0
DB2-1601	0.5	5.0e-5	5.0e-7	10.0	120	3.27e-2	9.81e-3
DB2-1701	0.5	5.0e-5	5.0e-7	3.5	120	1.87e-3	7.36e-3
DB2-1604	0.5	5.0e-5	5.0e-7	0	0	0	7.85e-3
DB2-1607	1.0	1.0e-4	1.0e-6	10.0	120	3.85e-2	1.67e-2
DB2-1608	1.0	1.0e-4	1.0e-6	3.5	120	2.34e-3	1.18e-2
DB2-1605	1.0	1.0e-4	1.0e-6	0	0	0	1.37e-2
DB2-1606	2.0	2.0e-4	2.0e-6	10.0	120	4.36e-2	2.94e-2
DB2-1603	2.0	2.0e-4	2.0e-6	3.5	120	2.16e-3	2.55e-2
DB2-1602	2.0	2.0e-4	2.0e-6	0	0	0	2.55e-2

[a]Calculated with the energy-based tidal power metrics and stress-based fluvial power metrics of Baumgardner (2015).

To increase the temporal efficiency of the experiments, a semicircular platform of sand-sized sediment was initially hand-laid to within 5 cm of the delta plain's intended starting elevation. Sea level was then raised and the remaining 5 cm were created by depositional processes from the point source until a delta topset of approximately 2 m radius was formed. To study how systems with established tidal networks respond to RSL rise, the first 3 hours of run time were allotted for tidal channel and network growth before RSL rise was initiated. This amount of time was deemed reasonable for acquiring a mature tidal network by looking at differential elevation between subsequent scans (Figure 2.2). In fact, areas of active erosion and deposition were readily identified between the first run hour and the third run hour. During the first hour the tidal channels were predominately erosional while some deposition occurred on the outer banks and as overbank deposits. Data from the third hour still showed erosion near the tidal channel inlets, with deposition in the seaward extent of the inlet, but the majority of the channels showed a net bypass stage with only minor net deposition on bends.

As the overall goal of this research is to understand how deltas of varying fluvial and tidal energy would respond to sea-level rise, consideration was given to decorrelate a delta system's response to RSL rise alone from its response to combined RSL rise and tides. Therefore, the amount of sediment discharge (Q_s) was set to maintain a 2 m radius shoreline in equilibrium with the rate of sea-level change, $\dot{H}_{SL}$, and the area, A_T, of the delta topset:

$$Q_s = \dot{H}_{SL} \cdot A_T / f \quad (1)$$

where *f* is the fraction of sediment discharge trapped in the topset. Here a value of 0.9 was used for *f* and was empirically chosen from test experiments conducted at SAFL. If a system was fluvial only with no tidal influence (DB2-1602, DB2-1604 and DB2-1605, see Table 2.1), the shoreline should remain static for the considered sea-level rise rate. Hence, any deviation in shoreline position or net deposition in experiments with active tides would be the result of tidal processes.

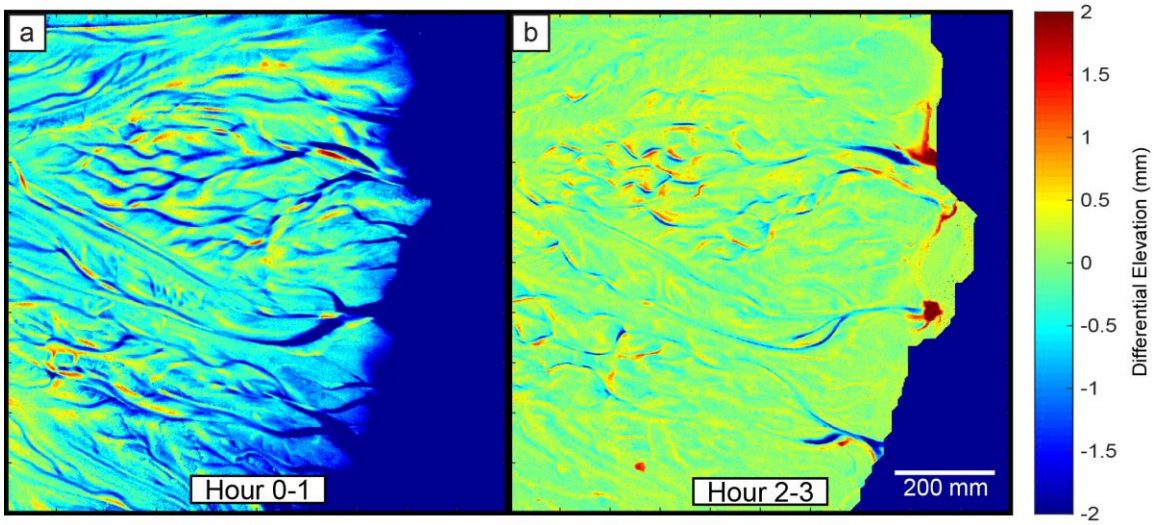

Figure 2.2: (a) Differential elevation between hour 0 scan and hour 1 scan. Tidal channels show clear development via erosion with deposition occurring on some outer banks and the delta plain between channels. (b) Differential elevation between hour 2 scan and hour 3 scan. Tidal channels still show some signs of erosion, although mostly at the tidal channel extremes: near the inlet and the headward extent. The mid-reach of the channels show very little activity and appear to be in a stage of net bypass while deposition is concentrated at the channel inlets.

3. EXPERIMENTAL RESULTS

3.1. Experimental and Field Geomorphic Similitude

The morphologies shaped in our experiments displayed several distinctive features of both tidal channel networks and of tide-influenced deltas. Channels shaped by the periodic action of tides start forming along the shoreline and progressively extend

toward the sediment source due to the progressive erosion of their headward extent driven by flow concentration during the ebb phase (D'Alpaos et al., 2005; Stefanon et al., 2010). Moreover, tidal channels showed a strong reduction in their width moving from the inlet toward the sediment source, thus resembling the classic "funnel-shaped" planform typically observed in tidal environments (Ahnert, 1960; Wright et al., 1973; Lanzoni and D'Alpaos, 2015) (Figure 2.2a). Furthermore, larger tidal channels tended to be straighter, while smaller channels were more sinuous, as is commonly observed in unvegetated tidal landscapes (Hughes, 2012). Overall, the tidal-channel networks produced in the experiments exhibited a dendritic structure, with maximum stream orders of about four or five according to Strahler's ordering (Strahler, 1957). These higher order channels were very persistent in the experiments and had a high preservation potential (Belknap and Kraft, 1985), especially if they remained segregated from active fluvial channels that could overprint smaller tidal features.

The delta morphology obtained from the experiments showed clear intertidal zones as identified from channel extents. Many of the longitudinal profiles captured in DEM data (Figure 2.3a), especially for tide-dominated experiments, show compound clinoforms (Figure 2.3b). Such features have been documented for major tidal delta systems such as the Ganges-Brahmaputra and Yangtze (Kuehl et al., 1997; Chen et al., 2000), and are typically associated with tidal acceleration which causes strong shear stresses on the inner shelf to form a region of limited deposition separating the subaerial and subaqueous clinoforms (Swenson et al., 2005; Goodbred and Saito, 2012). To the best of our knowledge, compound clinoforms have not been previously identified in any

experimental tidal deltas, marking our work as another benchmark for the capability of experimental systems to reproduce tidal morphologies and evolution in a realistic manner.

3.2. Shoreline Position

Monitoring shoreline migration through time provides suitable indicators of how deltas respond to sea-level rise, and it also marks an important boundary between fluvial and submarine transport processes, which has strong controls on not only the sedimentary structures but also on the preservation potential of stratigraphic sections (Swenson et al., 2000). Field stratigraphers solve an inverse problem when reconstructing ancient shorelines and often are faced with issues of stratigraphic completeness (Barrell, 1917; Sadler, 1981), which may necessitate modeling (Mahon et al., 2015). The physical experiments in this study allow for forward modeling and multi-dimensional tracking of shoreline trajectory at a high temporal resolution.

For our experiments, DEM data were the primary source of information for shoreline position. Starting near the sediment and water point source, topographic data in the form of longitudinal profiles was pulled in a radial pattern from 1° to 89° for a total of 89 profiles per hourly DEM scan (Figure 2.3). Not only did this allow for study of how the topset of the delta was evolving through time, but when coupled with controlled sea-level rise, the intersection of the current ocean level and profile gave the exact shoreline position at each time step.

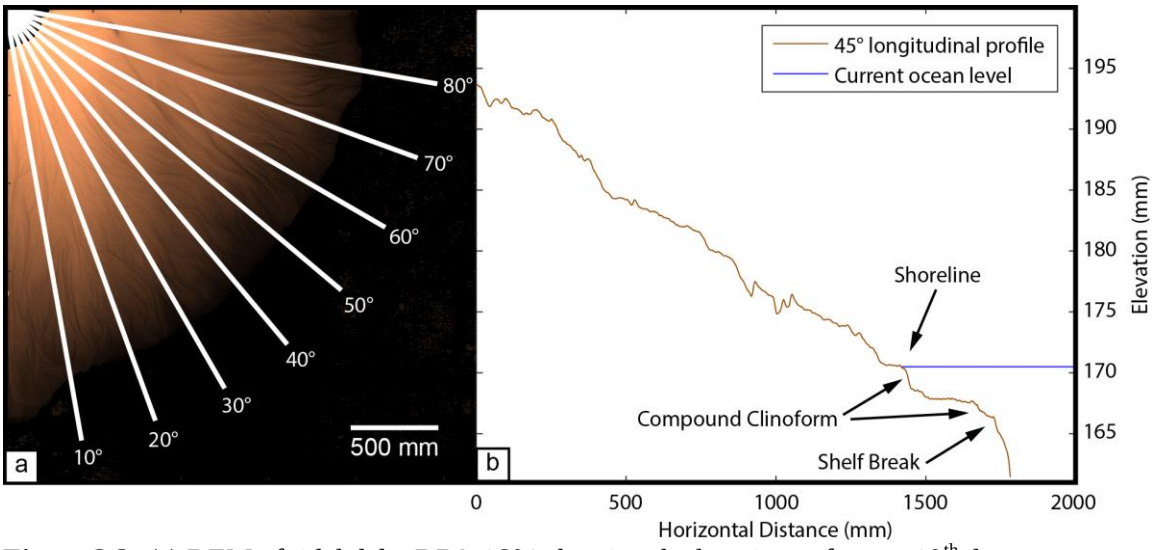

Figure 2.3: (a) DEM of tidal delta DB2-1601 showing the locations of every 10th degree longitudinal profile. Profiles were taken every degree from 1° to 89° and capture topset evolution. (b) An example profile taken from 45° showing the raw topographic data. Features that are identifiable include the shelf break as well as a compound clinoform. Using the current ocean level, the exact shoreline position was found and tracked throughout the experiment.

After each run hour, mean shoreline position was calculated from the 89 acquired shoreline positions across the delta (Figure 2.4). For a fluvial-dominated delta with no tides such as DB2-1604, the calculated sediment discharge was able to maintain an approximate shoreline radius of 2 m (Figure 2.4). The distributary network of channels efficiently distributed sediment across the delta throughout the rise in RSL. Both DB2-1602 and DB2-1605, which were purely fluvial experiments, started with a topset radius smaller than 2 m and their shorelines exhibited subsequent progradation of the delta (Figure 2.4).

In contrast to the fluvial experiments, for all the experiments involving tides, the mean shoreline position shows a transgressive delta, regardless if the delta is tide-influenced or tide-dominated. Experiment DB2-1600, which had no fluvial input, exhibits

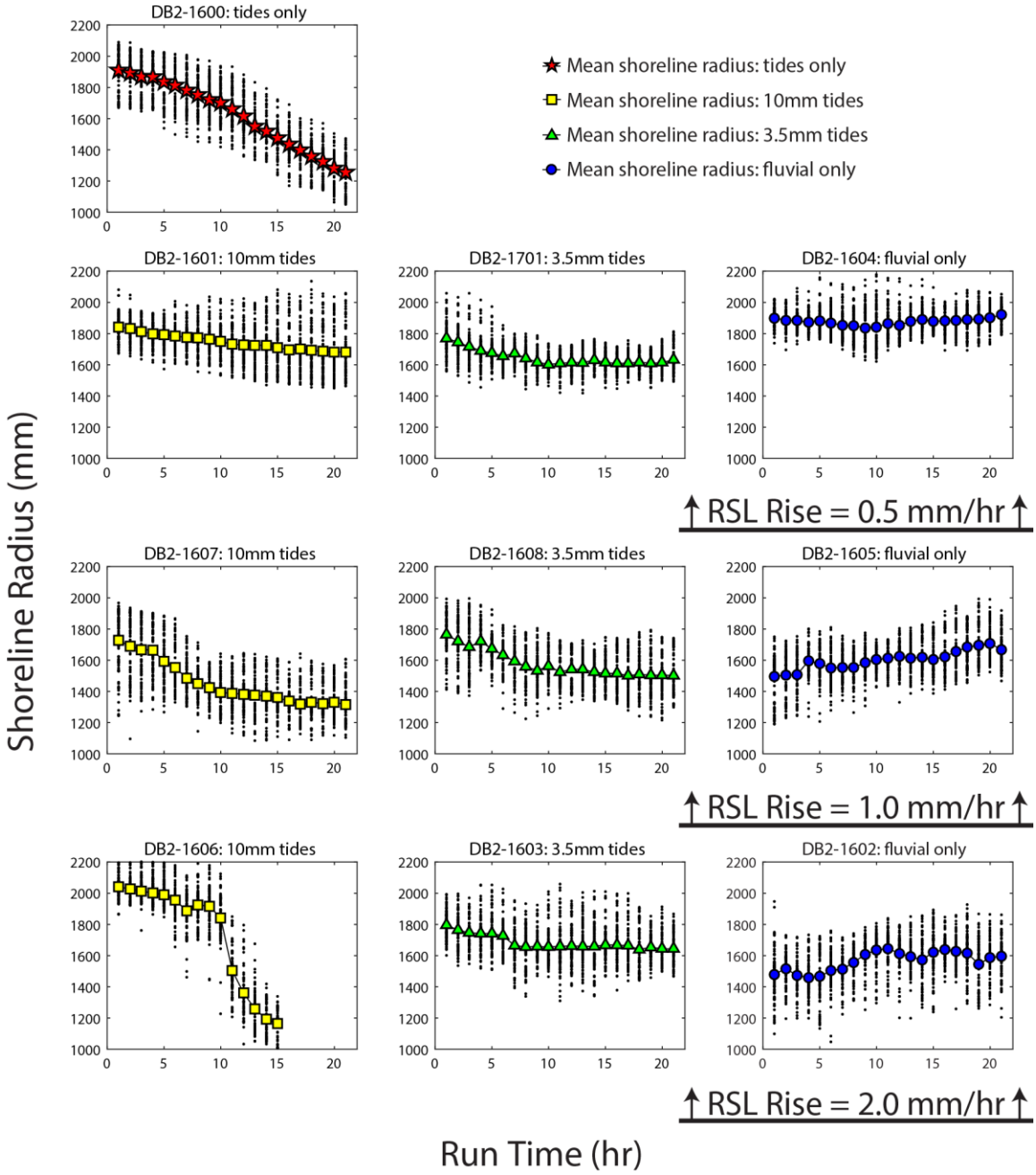

Figure 2.4: Shoreline position through time separated by relative sea-level rise rate. The shoreline was measured as a radius from the sediment and water point source and was plotted for 89 profiles taken every run hour. Mean shoreline position was also plotted to show the general shoreline migration trend. Refer to text for explanation of DB2-1606 results.

the highest rate of transgression, followed by tide-dominated systems (DB2-1601 and DB2-1607) and lastly by tide-influenced systems (DB2-1608 and DB2-1701) as seen in

Figure 2.4. Note that an error with the weir occurred during experiment DB2-1606 at run hour 9, causing a drop in sea-level. Subsequent erosion of the active distributary channel in DB2-1606 formed an embayment and the system transitioned to a tidal estuary. Although the issue was fixed at run hour 10, the fluvial system was well entrenched into the incisional valley feeding the embayment. This allowed for rapid transgression on the majority of the delta as the distributive channels could no longer deposit sediment to the now submerged portions of the delta plain and this is readily identifiable in the shoreline data (Figure 2.4).

3.3. Mean Profile Method

Observing how the shoreline evolves through time gives a general sense of how the delta is responding as a whole and implies conditions of nearshore sediment delivery or downstream depositional processes. The shoreline profiles shown in Figure 2.4 suggest that large amounts of sediment are being removed from systems with tides as the shoreline is able to transgress with little resistance. However, this does not explicitly capture net deposition metrics and gives no indication of the morphological adaption that takes place across the delta plain. Here we introduce a novel approach for comparing upstream and downstream net deposition along longitudinal profiles as well as creating metrics for comparison across delta systems. This “Mean Profile Method” (MPM) allows for the characterization of deposition and erosion along the same topographic profiles pulled for calculating shoreline and also quantifies the magnitude of net deposition.

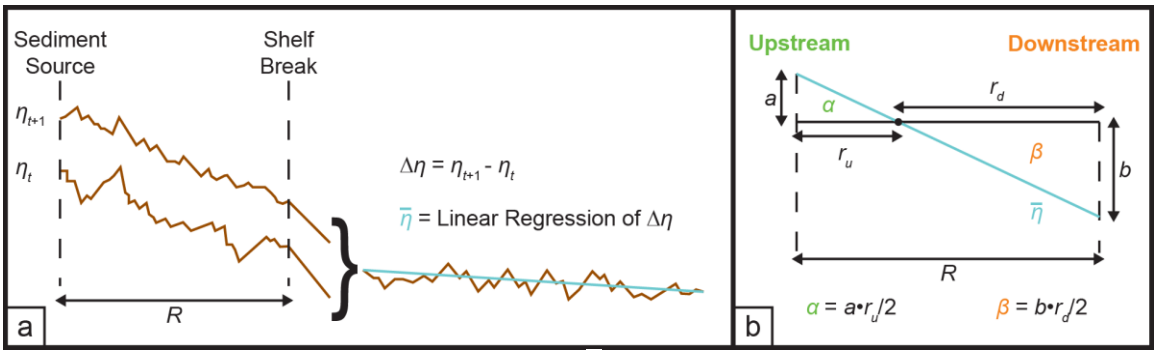

Figure 2.5: (a) Computation of the mean profile, $\bar{\eta}$. The difference, $\Delta\eta$, of two elevation profiles (η) taken at consecutive time-steps, t and t+1, is computed over the radius of the delta topset, R. The mean profile, $\bar{\eta}$, is finally computed as the linear regression of $\Delta\eta$. (b) Diagram depicting the variables employed to characterize the mean profile. A profile is divided into an upstream and downstream portion based on the position of the mean profile zero-crossing point. The upstream and downstream length, r_u and r_d, are then multiplied by half of the upstream and downstream depositional height, a and b, respectively to acquire the net upstream and downstream deposition areas, α and β.

The objective of the MPM is to compare subsequent topographic profiles to derive the differential elevation which captures the net deposition through time. For each delta, a series of topographic profiles, η_t, were assembled over time step t (Figure 2.5a). The difference in successive profiles through time, $\Delta\eta$, gives the absolute change in elevation. The linear regression of $\Delta\eta$ produces a simplified or mean profile, $\bar{\eta}$, which can be used to characterize upstream and downstream net deposition. The mean profile, which represents the interpolated elevation data, is separated into an upstream and downstream region based on the position of its zero-crossing point (i.e., the point where the mean elevation changes sign) (Figure 2.5b). Note that upstream and downstream classification of a region in this method does not imply a distinction in geophysical processes but instead serve purely as geographic distinctions. The distance from the sediment source to the zero-crossing point represents the upstream delta radius, r_u, while the remaining distance along the profile is designated as the downstream radius, r_d. The

elevation of the first and last points along the mean profile provide the upstream, *a*, and downstream, *b*, depositional heights respectively. Quite simply, these depositional heights are the maximum and minimum elevation values of $\bar{\eta}$. Finally, since the net depositional areas defined with this method are right triangles, the upstream and downstream net deposition can be found in units of area using:

$$\alpha = a \cdot r_u/2 \tag{2}$$

$$\beta = b \cdot r_d/2 \tag{3}$$

respectively, where the sign dictates positive or negative net deposition. As the initial delta geometry was set by deposition of sediment fed from the point source in the corner of the basin, each of the deltas started with different topset areas. To allow direct comparison of different experiments, α and β are normalized by the delta's initial topset area to obtain the dimensionless values α_* and β_*, which are then plotted in Cartesian space (Figure 2.6). As seen in Figure 2.6b, we can break the Cartesian space into octants numbered clockwise starting immediately north of the positive x axis, to represent different possibilities of net deposition captured by this method.

While several variations of the profile shown in Figure 2.5 are captured by equations 2 and 3, it is possible that there is no zero-crossing as the profiles show deposition or erosion along the entire profile (e.g., quadrants I and III in Figure 2.6b). In the case of uniform erosion or deposition along the profile (e.g., line of uniformity in Figure 2.6b), α and β are simply:

$$\alpha = a \cdot R/2 \tag{4}$$

$$\beta = b \cdot R/2 \tag{5}$$

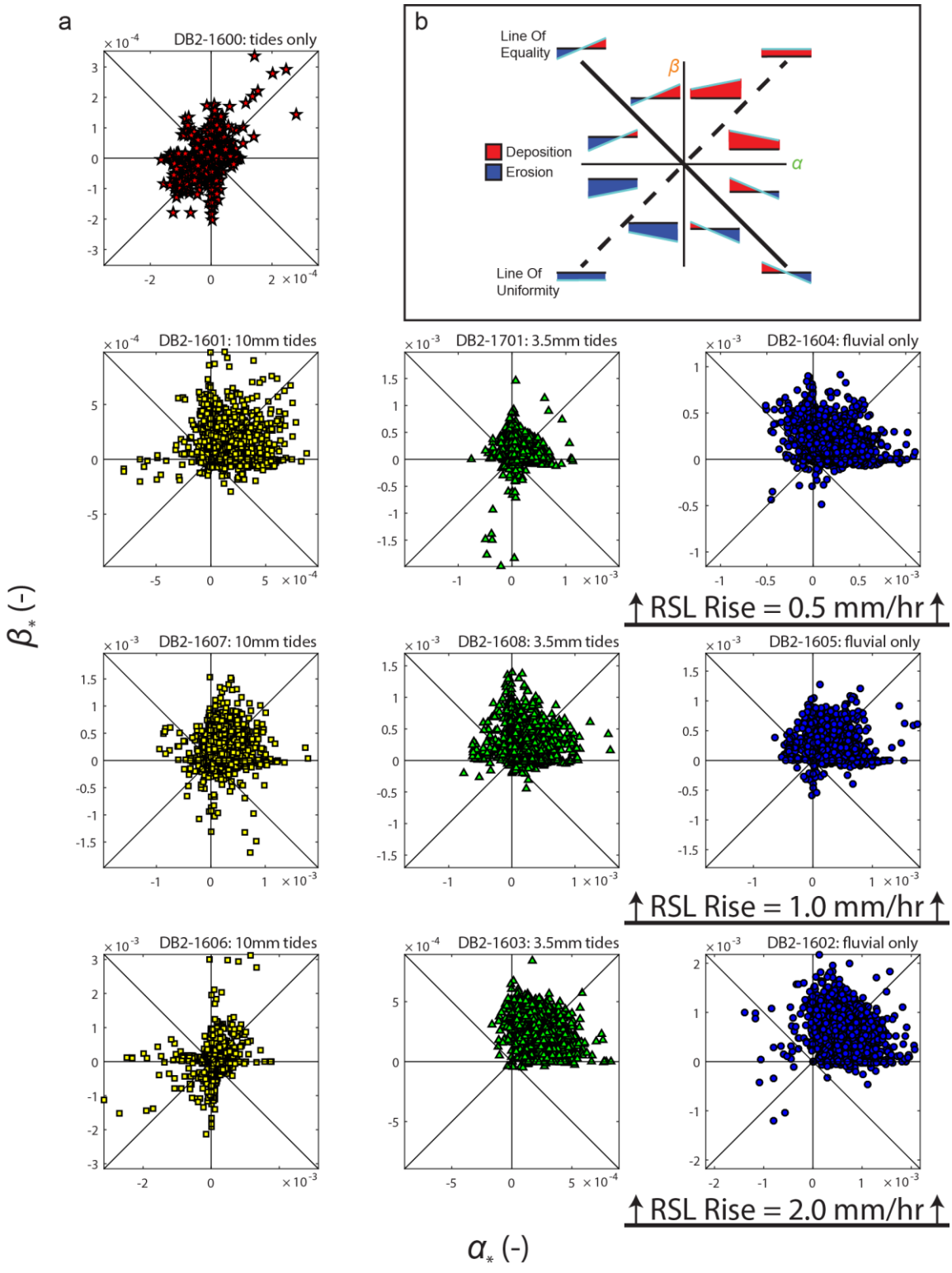

Figure 2.6: (a) Scatter plots of α_* and β_* separated by relative sea-level rise rate. α_* and β_* represent upstream and downstream net deposition respectively. The further away from the origin the greater the magnitude of net deposition. (b) A diagram depicting what each octant represents

in terms of net deposition profiles. Profiles alone the line of equality have equal upstream and downstream net deposition, while lines along the line of uniformity have uniform net deposition across the entire profile.

where R is the radius of the delta topset. This puts the separation of upstream and downstream at the center point of the profile. If deposition or erosion is not uniform across the profile, the upstream and downstream boundary is dependent on the magnitude of the depositional heights a and b. In these cases α and β are also found with equations 4 and 5, however instead of visualizing the areas as rectangles, the areas are again represented by right triangles. In this way, if a or b are small, their corresponding α and β values are small and the delineation of upstream and downstream is similar to how r_u and r_d were found. As a and b become closer to equal (e.g., line of uniformity in Figure 2.6b), the boundary of upstream and downstream migrates back to the center point and we again arrive at equations 4 and 5 with rectangles as our visualization for net deposition.

4. DISCUSSION

4.1. Shoreline Migration and a Transgression Anomaly

For purely fluvial experiments, sediment discharge rates calculated with equation 1 and shown in Table 1 were capable of either maintaining a pseudo-static shoreline radius (DB2-1604) or prompting a prograding radius (DB2-1602 and DB2-1605, see Figure 2.4). In marked contrast, every experiment with active tides produced a shoreline transgression, regardless of the ratio of fluvial to tidal energy for each system. The only difference between tide-dominated and tide-influenced systems, with all other parameters equal, appears to be the rate at which the shoreline regresses.

When tidal forcing is present, highly dynamic systems (i.e., systems experiencing higher RSL rise rates and sediment discharge) appear to transgress more quickly in some instances while about the same as less dynamic systems in others. When tides are absent, these same highly dynamic systems do not show transgression, implying that tides and their processes remove significant amounts of sediment from the delta plain. This also counter-intuitively suggests that tidal deltas are more sensitive to the rate of RSL rise, regardless of having a sediment budget large enough to combat eustatic rise under non-tidal conditions. This is in agreement with numerical modeling conducted by Van De Lageweg and Slangen (2017), who found that deltas are more easily inundated by higher rates of RSL rise irrespective of the ratios of fluvial, wave, or tidal energies acting upon them.

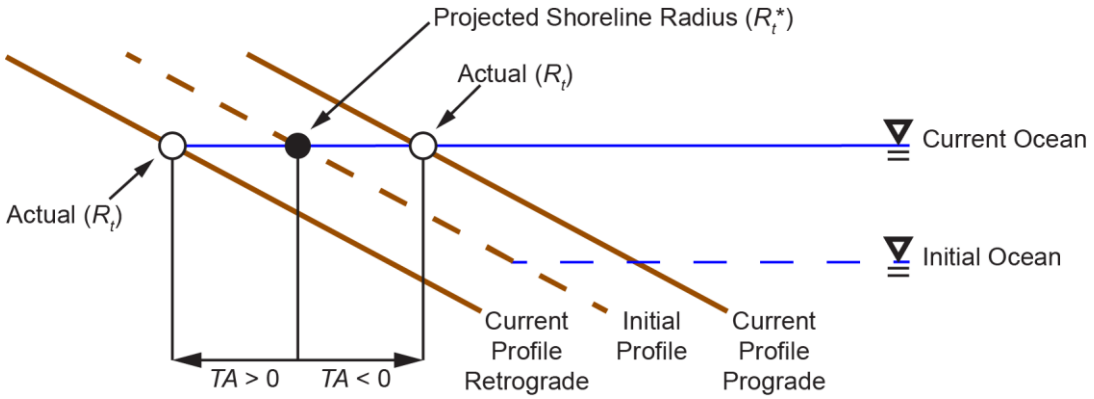

Figure 2.7: Schematic defining the transgression anomaly (*TA*). The projected shoreline position, R_t*, is based on the RSL rise rate and the initial delta plain profile while the actual shoreline position, R_t, is recorded from the intersection of the current profile and ocean level. If the current shoreline radius is larger than the projected radius the *TA* is negative, while shoreline radii that are smaller than the projected radius give positive *TA* values.

To further compare transgression rates between different experiments, it is beneficial to compare the actual evolution of shoreline position, R_t, with the position that

the shoreline would have maintained throughout the experiment if no depositional or erosional processes had occurred, R_t*. The latter is easily derivable by considering the intersection between the initial delta profile, assumed to be fixed, and the mean sea level at a given time step (Figure 2.7). Any difference between R_t and R_t* would reflect net deposition due to the action of fluvial and/or tidal processes. We therefore introduce a new metric, the transgression anomaly (*TA*), as:

$$TA = (R_t^*/R_t) - 1 \quad (6)$$

where systems that transgress faster than expected would have positive *TA* values and negative values for systems which transgress more slowly. Using the same 89 profiles per run hour from the shoreline data and the MPM, the initial profile was recorded from the first run hour and all subsequent shoreline positions were used to calculate the *TA* at each run hour. This gives 89 individual *TA* values for each run hour, which were then averaged to give one value for that time step (Figure 2.8).

When the transgression anomaly data is plotted (Figure 2.8), the magnitude of the *TA* value represents how far apart the current shoreline and the projected shoreline are in space. The experiment that involved only tides with no sediment input (DB2-1600) is the only system that shows TA values that are positive overall. Since net sediment flux in DB2-1600 is directed seaward, likely because flow concentration within channels during the ebb phase promotes stronger velocities - which in turn causes the system to be ebb-dominated, the shoreline transgressed more quickly than predicted by the initial profile. When any rate of sediment discharge is introduced, the systems show negative *TA* values on average, which indicates aggradation and/or progradation along the delta topset.

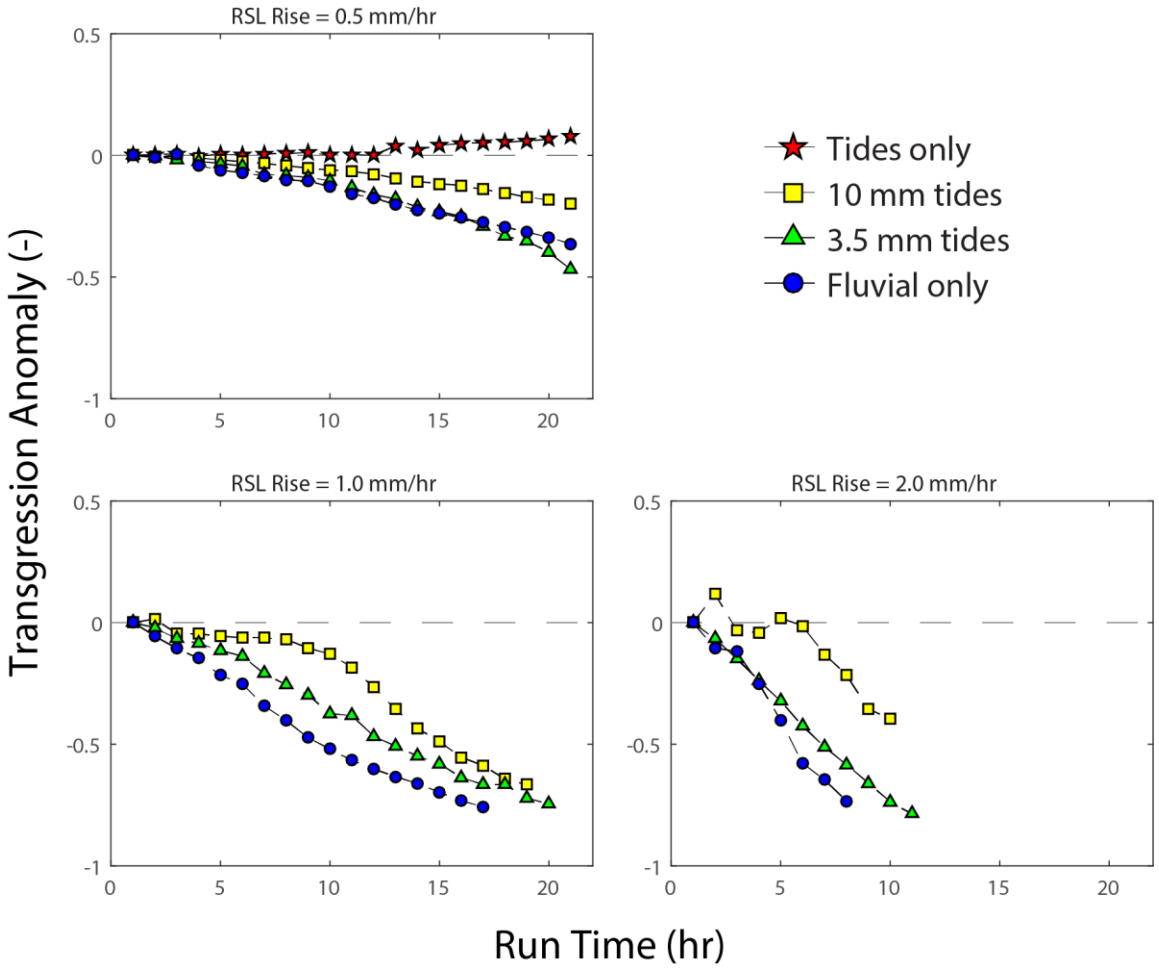

Figure 2.8: Transgression anomaly (*TA*) vs. run time separated by relative sea-level (RSL) rise. Note that while all experiments were run for 20 hours, profiles in the faster RSL rise rates terminate before the last run hour. This is due to how the *TA* is calculated; the initial profile would be completely flooded by these times and the *TA* can no longer be used. The difference in how long this takes between systems is dependent on the initial topset slope.

As the rates of RSL rise and sediment discharge increase in these experiments, the slopes of the connecting lines become steeper. This implies that while the shorelines in these highly dynamic systems do ultimately transgress (Figure 2.4), they do so at a lower rate than systems with no sediment input. The systems that were subjected to high RSL rise rates of 2 mm/hr (DB2-1602, DB2-1603 and DB2-1606) also had higher sediment and water discharge rates, which produces a fluvial system with higher energy (Table

2.1). As fluvial energy in the system increases, the ability of tides to increase transgression rates decreases. Conversely, higher tidal energies lead to higher transgression rates over systems with comparable sediment budgets.

The *TA* dataset implies that the response of dynamic delta systems may be harder to predict when based solely on initial conditions. The addition of tidal forcing further complicates the morphologic response of a delta as fluvial processes of deposition are clearly interrupted when observing the shoreline and *TA* data. The ebb phase of the tide dominates on these deltas and irrespective of the relative energy of the tides, sediment that would otherwise be deposited in the topset is instead transported to the foreset, bottomset or the representative deep marine.

While it is possible that tidal deltas that are vegetated or flood-dominant would respond to RSL rise differently, calculations of sediment budgets for several of the world's tidal deltas show large amounts of sediment transported to the subaqueous delta clinothems. Early calculations for the sediment budget of the Fly delta could only account for half of the annual sediment load within the tide-dominated regions (Harris et al., 1993). It was later discovered that while some of the missing annual sediment budget is deposited on the Fly river's floodplain (Swanson et al., 2008), a large portion is appropriated to a composite clinothem forming the inner Gulf of Papua shelf (Slingerland et al., 2008). A similar study of the Ganges-Brahmaputra by Goodbred and Kuehl (1999) found that two-thirds of the annual sediment discharge is sequestered by the prograding subaqueous delta and the deep-sea Bengal fan. Studies of the major East Asian tide-dominated and tide-influenced deltas have shown that not all sediment removed from the

subaerial delta plain is redeposited in the immediate alongshelf clinothem. In fact, 25-35% of the sediment load in these delta systems is transported between 500-800 km alongshore before final disposition in a shore-parallel middle-shelf clinothem (Liu et al., 2009). This complex picture of continental margin deposition only highlights that several components may work in conjunction with tides to enhance sediment flux seawards. However, since these experiments are ebb-dominant, they lack a significant landward component of suspended sediment transport. Tidal channels downdrift of distributary channels with high suspended sediment concentrations have been shown to deliver fines onshore if tidal currents are flood-dominant, as is the case in several of the north-south trending tidal channels west of the Ganges-Brahmaputra-Meghna river mouth in the Bay of Bengal (Barua, 1990; Barua et al., 1994). Therefore, our results that show net-export of sediment may reflect dominantly bedload sediment transport.

4.2. Profile Preference and Net Deposition

As seen in Figure 2.6, the Mean Profile Method is able to capture delta plain evolution in terms of net deposition and its morphologic response. With the exception of DB2-1600, which had no sediment input, the majority of topographic profiles plot in octants that correspond to positive net deposition (Figure 2.6). However, the capturing of sediment in topsets of tidal delta systems does not outpace accommodation space created by RSL rise. As seen in the tide-dominated and tide-influenced shoreline and transgression anomaly data, transgression occurs in all tidal systems (Figures 2.4 and 2.8). Using the fluvial only delta systems as a baseline, the axes values give a sense of how much α_* and β_* values increase as the delta systems become more dynamic. For each

bracket of RSL rise, the magnitude of upstream and downstream area change also tends to increase as the system becomes less tide-influenced. This trend appears to show that tides reduce the net deposition occurring on the delta topset. Therefore, the MPM data correlates well with the trends seen in the shoreline and TA data and again points to sediment bypass occurring within the delta plain.

While the scatter plot of Figure 2.6 captures the direct results of the MPM, the volume of data produced is better represented with a rose diagram. Often used to represent wind direction and frequency, here the direction shows which octant the data lies in and the percentage of profiles in that octant (Figure 2.9). Lastly, the distance from the origin to the data point represents the magnitude of area change in the MPM and is represented in the rose diagram with color. The diagrams shown in Figure 2.9 elucidate the results of the MPM and show a clearer transition in depositional response from low sediment/low RSL rise systems to more dynamic systems.

Observing Figure 2.9, the tides-only delta system (DB2-1600) shows mostly erosion dominated profiles, although approximately 25% of the profiles show upstream deposition (octants 7 and 8) with 10% being upstream deposition dominant (octant 8). Therefore even though tidal deltas created in DB-2 are ebb-dominated, the subordinate currents in the flood phase still have the capability of depositing sediment along tidal channel apexes. When sediment carrying fluvial channels are introduced, there is a strong transition to upstream dominant deposition and downstream erosional profiles (octant 8). For deltas experiencing 0.5 mm/hr of RSL rise (DB2-1600, DB2-1601, DB2-1604 and DB2-1701), as the fraction of fluvial power to tidal power increases there is a small

transition (~5%) to upstream erosional and downstream dominant deposition (octant 3). It is possible that upstream scour at the point source is responsible for this small conversion of profiles as tide-influenced deltas created a slight slack water near the point source during high tide. This slack water condition allowed for increased deposition of suspended sediment which helped mitigate local scour.

The delta systems exposed to 1.0 mm/hr of RSL rise (DB2-1605, DB2-1607 and DB2-1608) show an overall decrease in upstream dominant deposition and downstream erosional profiles (octant 8) as the systems transition to profiles in the first quadrant which are depositional along the entire profile. Again as these delta systems become less tide-influenced there is a slight increase in the number of profiles that show upstream erosion and downstream dominant deposition (octant 3). Finally, the systems with RSL rise rates of 2.0 mm/hr (DB2-1602, DB2-1603 and DB2-1606) have almost all profiles in the first quadrant of deposition up- and downstream with the exception of DB2-1606 which created an estuary style embayment. The tide-influenced delta (DB2-1603) showed slightly more profiles which were downstream dominant depositional (octant 2) and the fluvial only delta (DB2-1602) showed the opposite with slightly more upstream dominant depositional profiles (octant 1).

Not only do the delta systems vary in their preferred profiles as they become more dynamic, but the average net area change increases overall as more sediment and accommodation space is introduced. Although DB2-1600 had 10 mm amplitude tides, the net area change is the smallest as no source of sediment exists. Conversely, the delta

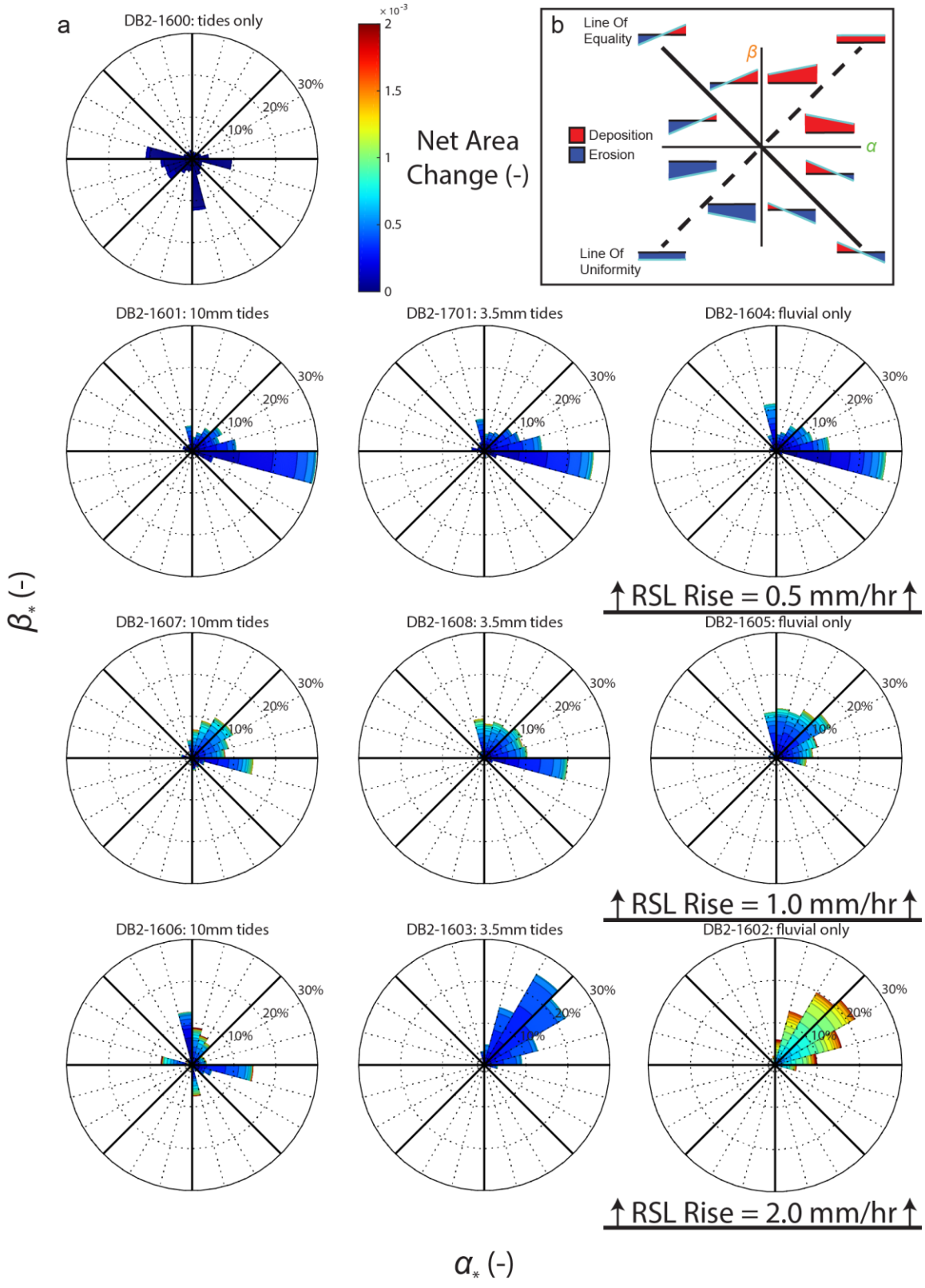
a
DB2-1600: tides only
× 10^-3
2
1.5
1
0.5
0
Net Area Change (-)
b
Line Of Equality
β
Deposition
Erosion
α
Line Of Uniformity
DB2-1601: 10mm tides
DB2-1701: 3.5mm tides
DB2-1604: fluvial only
RSL Rise = 0.5 mm/hr
DB2-1607: 10mm tides
DB2-1608: 3.5mm tides
DB2-1605: fluvial only
RSL Rise = 1.0 mm/hr
DB2-1606: 10mm tides
DB2-1603: 3.5mm tides
DB2-1602: fluvial only
RSL Rise = 2.0 mm/hr
30%
20%
10%
β* (-)
α* (-)

Figure 2.9: (a) Rose diagrams of α_* and β_* for different relative sea-level rise rates. Percentages represent frequency of profiles falling within a certain octant. Color depicts the net area change which is also how far the α_* and β_* values, which are proxies for upstream and downstream deposition respectively, plot from the origin (b) A diagram depicting what each octant represents in terms of net deposition profiles.

systems with the highest sediment discharge and RSL rise rates have profiles with the highest net deposition. Comparing DB2-1602 and DB2-1603 gives a sense of how much net deposition needs to occur to outpace RSL rise. DB2-1602, which was a fluvial only delta that prograded, has the largest values of net deposition. DB2-1603, which had the same sediment discharge rate but also had 3.5 mm tides, experienced transgression and shows less overall net deposition.

A parallel exists in these delta systems between the recorded magnitude of the transgression anomaly and the magnitude of net area change. The deltas that had *TA* values closer to zero show the smallest net deposition while the opposite is true for deltas that diverged the fastest and furthest from a zero *TA* value. While highly dynamic deltas seem to be more suited to counteract the effect of RSL rise, tidal influence in these systems ultimately allowed for a transgression to occur. This coincides with delta research of very energetic river mouths, such as the Amazon (Kuehl et al., 1986) and Fly (Harris et al., 1993) which show delta growth primarily in the form of a subaqueous mud clinoform leaving the subaerial delta susceptible to transgression. Both of these delta systems are subjected to tidal forcing and it is believed that tidal focusing inhibits sediment accumulation on the delta topset (Nittrouer et al., 1986; Allison, 1998).

In contrast to most modern deltas, research on the very dynamic Ganges-Brahmaputra delta has shown that the subaerial delta front has prograded over the last

200 years in the face of Holocene sea-level rise (Allison, 1998; Akter et al., 2016). This draws attention to several factors present in that system as compared to these experimental deltas. Chief among them is the lack of vegetation on the delta top and absence of multiple grain sizes. Vegetation found in mangroves and salt marshes in particular interact with fine grained clastics to promote the capture of suspended sediment. While these inclusions may account for the lack of transgression in the Ganges-Brahmaputra Delta, some of the tide-dominated experiments shown here do replicate the composite nature of the Ganges Delta.

For example, DB2-1606 (10 mm tides with 2 mm/hr RSL rise) is unique as it is the only experiment that indicates how a delta experiencing regression and valley-style erosion responds to subsequent transgression. The majority of expected profiles for the other delta systems fall in octants 1, 2 and 8 with less than 10% also in octant 3. However, as all of the fluvial discharge was trapped within the embayment, a large portion of the delta was influenced by tides only, which created profiles in octants 4 and 7. Accounting for roughly 16% of the total profiles, these are upstream dominant erosional and downstream depositional (octant 4) and upstream depositional and downstream dominant erosional (octant 7). Profiles from these portions of the delta are directly comparable to the majority of profiles found in DB2-1600 which was a delta system with only tides and no fluvial input. Therefore, different areas of DB2-1606 show parity to multiple delta types as different processes dominated in these sections.

Field studies of asymmetric wave-influenced deltas (e.g., Danube and Brazos deltas) have shown differences in sedimentary facies updrift and downdrift of the main

channel outlet. Bhattacharya and Giosan (2003) believe this variation is due to several modifying processes active in the downdrift area such as lagoonal, lacustrine, fluvial, tidal and vegetation-related sedimentation. More recently, large deltas can be considered a composite system if different portions are controlled by fluvial, tidal or wave processes which give distinctive morphologies across the delta (Goodbred and Saito, 2012). Although DB2-1606 is unique in that it was the only experiment that behaved as an estuary, it was not the only delta system to show varying topset morphologies.

4.3. Composite Deltas

During the entirety of experiment DB2-1601, a tide-dominated delta experiencing a steady 0.5 mm/hr RSL rise, the main distributary channel was pinned to the delta's northernmost boundary by the strong 10 mm amplitude tides. Periodically a smaller secondary channel would branch off from the main channel and attempt to fill in the accommodation space being created throughout the delta. As a mature tidal network was already formed on the remaining delta plain, a unique interaction between the secondary fluvial channel and the tidal network existed. Distributary channels would preferentially meet the headward extent of the tidal channels and evacuate their sediment load down the channel with very little overbank deposition. The relationship between the fluvial and tidal systems in DB2-1601 led to the development of a composite delta system with varying tidal and fluvial morphologies seen across the delta.

The delta can be qualitatively discretized into four regions based on the varying influences of tides and fluvial channels. The area where the main distributary channel was pinned during the entirety of the experiment we classified as fluvial dominated. The

immediate flanks of this channel were classified as fluvial influenced. Regions where the tidal forcing appeared to outweigh fluvial influence, we identified as tide influenced, and where the tidal network rarely interacted with distributary channels, we named tide dominated. Using these four regions, shoreline position, transgression anomaly and mean profile method data can be compared (Figure 2.10).

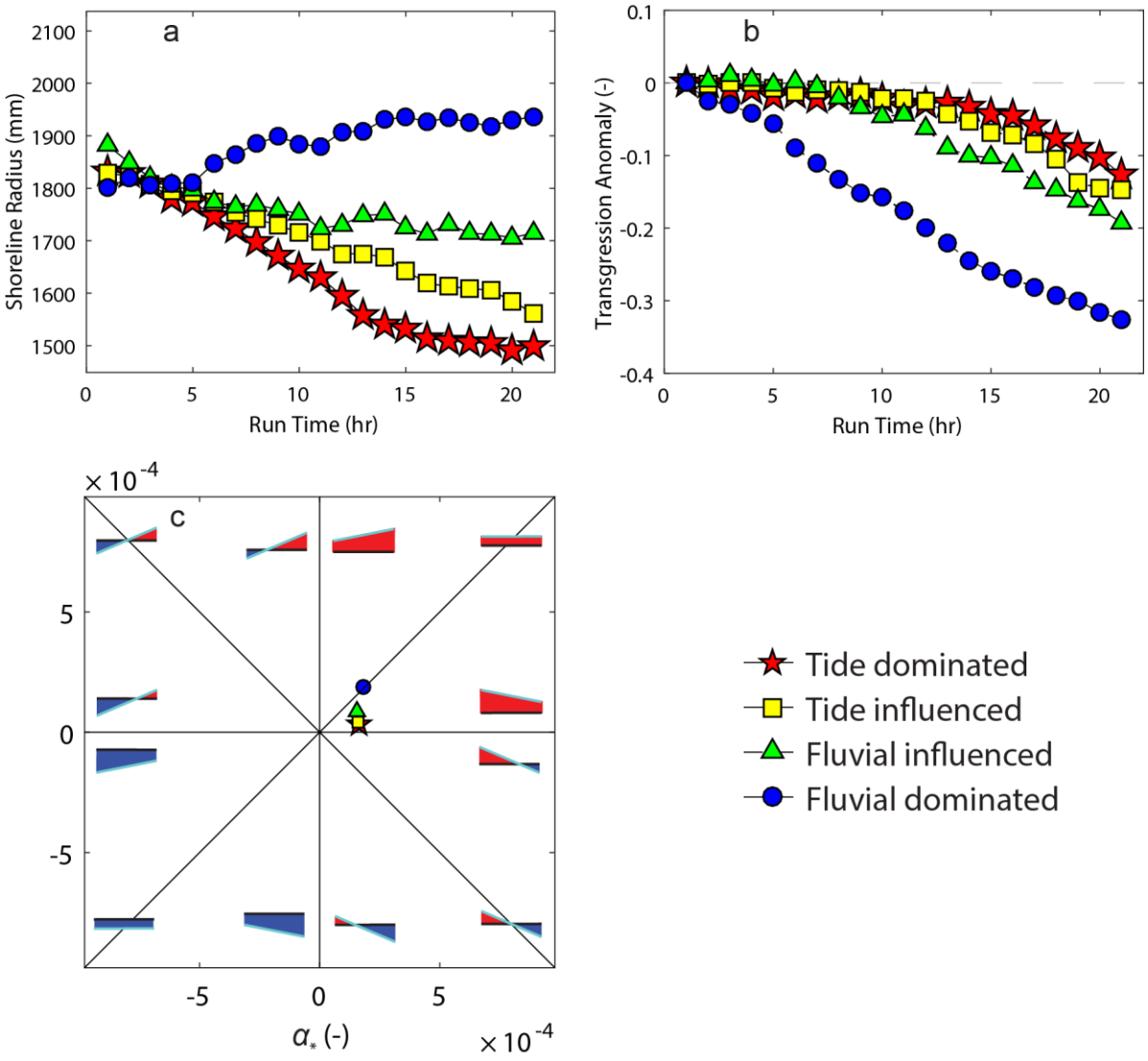

Figure 2.10: Composite delta data for DB2-1601: 10mm tides. The delta was separated into four regions based on the observed influence of fluvial vs. tidal processes. (a) Mean shoreline position through time for each region. (b) Transgression anomaly (*TA*) through time for each region. (c)

Scatter plot of mean α_* and β_* values for each delta region to indicate the preferred net depositional profile.

While the selection of these areas was based on observation, the shoreline position and transgression anomaly values fall in line with the observed results seen across experiments with varying tidal and fluvial energies. As fluvial power decreases, transgression of the shoreline increases and the *TA* moves closer to values of zero (Figures 2.10a and 2.10b). For the MPM, the mean α_* and β_* were plotted to show the preferred profile for each section (Figure 2.10c). This preferential profile transitions from upstream deposition dominant and downstream depositional (octant 1) to roughly uniform upstream and downstream deposition as the fluvial system becomes the dominant force. These results display the ability of physical delta models to morphologically replicate composite delta environments. As experimental delta facilities continue to evolve, improved modeling of marine processes will improve our understanding of composite deltas.

5. CONCLUSIONS

The experiments presented here have shown that physical models of tidal environments can be extended to depositional systems such as deltas. These results open an avenue of experimental research that previously focused on systems such as estuaries and gives credibility to the recorded response of these tidal deltas to the allogenic forcing of RSL rise. While several complexities found in the field such as multiple grain sizes, vegetation and flood dominant currents are not included, we believe these experiments provide a baseline for comparing the response between fluvial- and tide-dominated delta systems to eustatic variation. Furthermore, using DEM data in the form of longitudinal

profiles, we have shown the transgression anomaly to be a useful method for comparing shoreline transgression between deltas experiencing different rates of RSL rise. The usefulness of these profiles is further exemplified by a newly developed mean profile method, which not only simplifies upstream and downstream deposition profiles, but uses the normalized area change between subsequent profiles as a metric for net deposition. Based on our results generated from these new methods, we find that:

(1) Tidal deltas show transgressive shorelines, regardless of tidal strength, under conditions in which fluvial deltas show shoreline stasis or regression;

(2) The most dynamic fluvial-dominated delta system showed longitudinal profiles with up to two times the net deposition found in its tide-dominated and tide-influenced counterparts pointing to sediment removal by tides;

(3) As tidal delta systems become more dynamic (i.e., high sediment discharge and high RSL rise rates), they transition from predominately upstream deposition and downstream erosion to up- and downstream deposition;

(4) Strong tidal forcing can immobilize distributary channels and leads to composite delta morphologies as tidal and fluvial processes dominate different regions of the delta.

While all of the world's deltas are vulnerable to sea-level fluctuations due to their low gradients, as seen here tides can potentially compound the local effect of sea-level rise as their cycle amplifies the mean eustatic trend. Going forward, new consideration must be given to the effectiveness of sediment removal in delta systems affected by ebb-dominated tidal currents. We believe that these initial findings improve our current understanding of tidal delta evolution and this in turn should allow for more comprehensive and accurate modeling of these dynamic depocenters, an increasingly important tool as modern sea-level continues to rise, threatening these populous deltas.

NOTATION

Q_s	sediment discharge (m^3/s)
$\dot{H}_{SL}$	rate of sea-level change (mm/hr)
A_T	area of delta topset (mm^2)
f	fraction of sediment discharge trapped in delta topset
η_t	topographic profile at time step t
t	time step (hr)
$\Delta\eta$	difference in successive topographic profiles
$\bar{\eta}$	linear regression of $\Delta\eta$
r_u	upstream radius (mm)
r_d	downstream radius (mm)
a	upstream depositional height (mm)
b	downstream depositional height (mm)
α	area of upstream net deposition (mm^2)
β	area of downstream net deposition (mm^2)
α_*	α normalized by initial topset area (-)
β_*	β normalized by initial topset area (-)
R	radius of the delta topset (mm)
R_t	actual shoreline position (mm)
R_t*	projected shoreline position (mm)
TA	transgression anomaly (-)

3

Reduction of deltaic channel mobility by tidal action*

*****Submitted as Lentsch, N., Finotello, A., and Paola, C. *Reduction of deltaic channel mobility by tidal action* to Geology.

SYNOPSIS

As Holocene river deltas continue to experience sea-level rise, they use sediment carried by distributary channels to counteract delta-plain drowning. Many deltas worldwide are subjected to tidal action, which strongly affects the morphodynamics of distributary channels and could also influence their mobility. Here we show, through physical laboratory experiments, that distributary-channel mobility can be dramatically reduced in systems affected by tides in comparison to an identical system with no tides, and that the mobility of distributary-channels decreases as the ratio of tidal to fluvial energy increases. We also show, using a new approach to create synthetic stratigraphy by coupling digital elevation model data and time-lapse photography, that the decrease in distributary-channel mobility in tide-influenced deltaic systems increases channel stacking and connectivity.

INTRODUCTION

Deltaic environments support productive coastal ecosystems and large human populations, with the tide-influenced megadeltas of Asia (e.g., the Ganges-Brahmaputra, Mekong, Changjiang, etc.) alone hosting over 200 million humans (Woodroffe et al.,

2006; Goodbred and Saito, 2012). Understanding how these deltas respond morphologically to rising relative sea level is therefore critical for managing the evolving landscape and the population it supports. While there are numerous examples of modern tidal deltas, the study of ancient deposits allows a long-term view of the evolution of delta morphology (Blum and Törnqvist, 2000). However, tidal deltas are difficult to identify definitively from the stratigraphic record and few clear examples have been recognized in the rock record (Plink-Björklund, 2012): some key morphological indicators, such as tidal mouth bars and funnel shaped tidal channels, are not readily identifiable in ancient deposits (Dalrymple and Choi, 2007). Physical experiments (Malverti et al., 2008; Paola et al., 2009; Kleinhans et al., 2012) offer an additional source of insight allowing, for example, study of processes such as distributary-channel mobility at a temporal and spatial resolution that is impractical in the field.

While recent studies with tides in physical experiments have successfully created tidal networks (Vlaswinkel and Cantelli, 2011; Kleinhans et al., 2012) and estuaries (Kleinhans et al., 2014), their focus was not on depositional distributive networks. Distributary channels are crucial to understanding the eco-morphodynamic evolution of deltas as they are the main conduits through which water, sediment and nutrients propagate. Channel mobility is thought to be strongly influenced by localized sedimentation (Bridge and Jarvis, 1976; Pizzuto, 1987; Slingerland and Smith, 1998; Hajek and Edmonds, 2014). However, little is known about the effect of tides on channel mobility, though their morphologic effects have been explored since the fundamental work of Galloway (1975), and expanded upon by Nienhuis et al. (2015). While there

have been advances in modeling nearshore processes and their effects on distributary-channel mobility (Swenson, 2005), the overall effect of tidal action on distributary channel mobility, and its stratigraphic record, are not well understood.

Here we present the results of experiments carried out at Saint Anthony Falls Laboratory (SAFL) to investigate how tidal forcing affects morphodynamic and stratigraphic evolution of deltas under depositional conditions. Specifically, we investigate how tides influence channel mobility by varying total tidal energy relative to fluvial energy. We combine data from time-lapse photography and high resolution digital elevation models (DEM), using a new procedure, to derive two types of *in situ* synthetic stratigraphy. We first describe the experiments and data collection; we then quantify the mobility of distributary channels subjected to varying tidal energies and use synthetic stratigraphy to compare channel body distribution and connectivity. Our results show that tides significantly reduce the mobility of distributary channels in deltaic systems.

METHODS

We conducted a series of delta experiments at SAFL in a 5 m x 5 m x 0.5 m basin with a computer-controlled system that allows for continuously varying water and sediment inputs, and programmable changes in base level. The latter is regulated via an electrically operated weir, while sediment and water are supplied by a feed system in one corner of the basin. The basin is unique in that it also can produce sinuous tides via two large pumps connecting the main basin to an auxiliary basin. More information on the experimental setup, is in the GSA Data Repository[1] (Fig. A.1).

Three delta experiments are the focus of this study; their varying tidal parameters can be found in Table 3.1 (Table A.1 in the GSA Data Repository[1] contains information on supplemental experiments). Prior to each experiment, we grew an approximately uniform 2 m radius delta using walnut-shell sand (D_{50} ~ 320 μm) that, owing to its low density (1350 kg/m^3), can be easily entrained and deposited by both tidal and fluvial currents (Baumgardner, 2015). Then we imposed a steady relative mean-sea level rise that continued for the whole experiment. Sediment and water discharges were set to keep pace with base-level rise, maintaining a constant delta-topset area. To isolate the effects of tides on distributary-channel mobility, base-level rise and sediment and water discharge are constant while tide parameters vary for each experiment.

TABLE 3.1 EXPERIMENT PARAMETERS AND ENERGIES

Experiment	Tide Amplitude (mm)	Tide Period (sec)	Tidal Power (W/m)*	Fluvial Power (W/m)*	Total Aggradation (mm)
DB2-1601	10.0	120	3.27e-2	9.81e-3	10.0
DB2-1701	3.5	120	1.87e-3	7.36e-3	30.0
DB2-1604	N/A†	N/A†	N/A†	7.85e-3	10.0

Note: Sediment discharge (5e-7 m^3/s), water discharge (5e-5 m^3/s) and base-level rise (0.5 mm/hr) are the same for all experiments and were held constant throughout each.

*Calculated with the energy-based tidal power metrics and stress-based fluvial power metrics of Baumgardner (2015).

†N/A = not applicable.

The main observations during each run were overhead time-lapse imaging every 3 mins for DB2-1601 and 1 min for DB2-1604 and DB2-1701, and high resolution (<1 mm vertical, 1 mm horizontal) topographic scans (DEM), taken every hour. Data analysis focused on (1) measuring how changing relative tidal strength influenced channel mobility, and (2) measuring how changes in mobility were recorded stratigraphically. We adopted a method similar to Wickert et al. (2013) and Baumgardner (2015) in which channel mobility is measured by change in wet/dry pixel state between sequential images.

These state changes are normalized by the number of common pixels in both images to give a state change fraction, which is then divided by the time step between images to compute the state change fraction per time (Fig. 3.1). We then use mean state change fraction per time ($\overline{M}$) values to compare channel mobility between experiments.

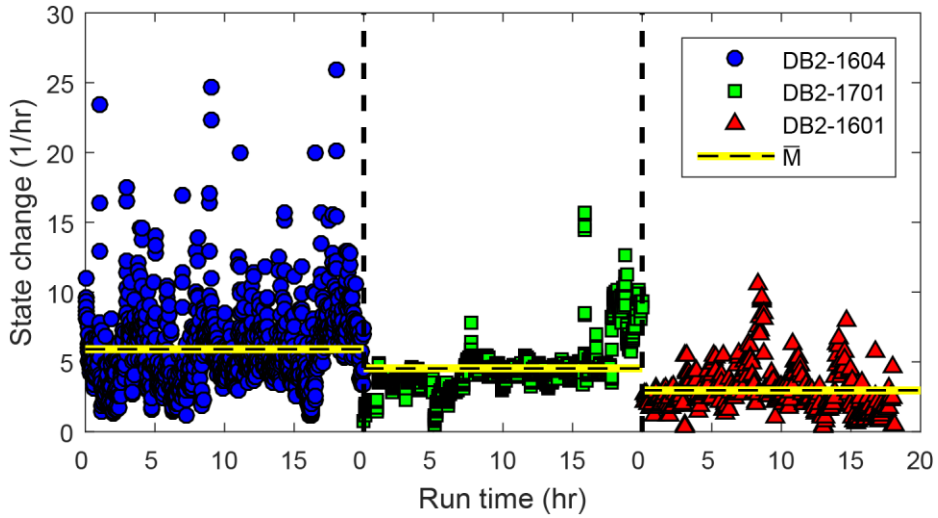

Figure 3.1: State change in pixel fraction per time versus run time for all three experiments. Each data point represents the change in "wet" and "dry" pixels for consecutive images which is used here as a proxy for channel mobility. Spikes in the plotted data are associated with avulsions which see rapid rates of change as a channel is abandoned in favor of a new flow path. Mean state change fraction per time for the entire experiment ($\overline{M}$) is calculated for each and is a quick reference for overall channel mobility across delta systems. Note the missing data points for the last two hours of DB2-1601 as the marker dye ran out; they are not used when calculating $\overline{M}$.

To study the stratigraphic signature of changes in channel mobility, we need to visualize the buried channels. Unlike previous experiments that preserved well defined channel bodies in cross-section (Kim et al., 2006; Sheets et al., 2007), the well-sorted, low-density sand we used does not yield visible buried channels. To compensate, we used the images and DEMs to construct synthetic stratigraphy along a given transect on the delta top. Since the focus of the present work is on distributary channels, we focused on one topographic transect located just outside the intertidal zone (Fig. 3.2A). As for the

DEM data, to reduce noise and aid in identifying channels, we applied a Savitzky-Golay filter, which preserves relevant high frequency components of the data (Schafer, 2011), to each transect profile. The filter has a window of 50 data points (corresponding to 50 mm) and its coefficients are specified by a 2nd degree polynomial via unweighted linear least-squares regression. After filtering, we plot elevation data along the transect for each hourly scan with subsequent topography clipping previous values wherever the later elevation is lower (Fig. 3.2B).

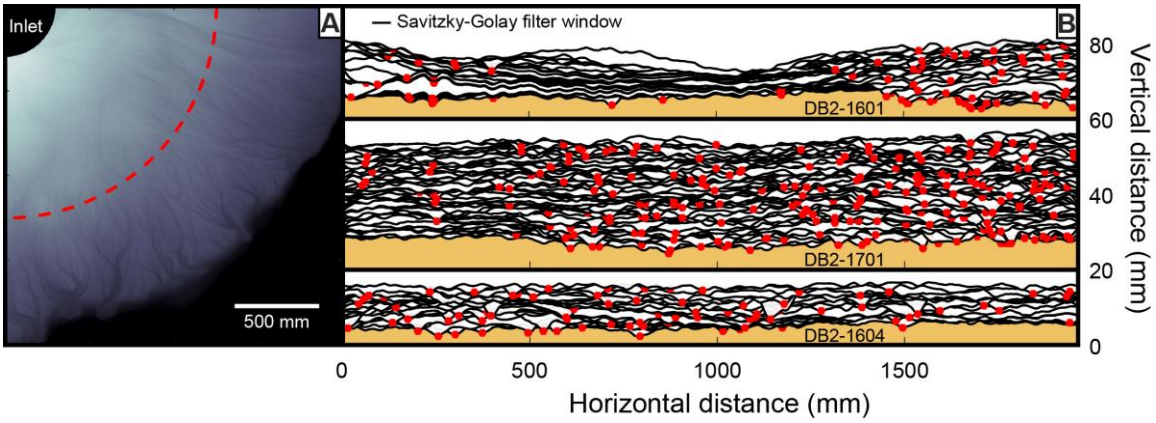

Figure 3.2: A: DEM image of experiment DB2-1601 with several tidal channels evident. The red-dashed line indicates the transect location for the generated synthetic stratigraphy. B: Synthetic stratigraphy where each horizon depicts the topography at an hourly DEM scan. Subsequent scans clip lower elevations to represent areas of erosion. All topographic profiles were smoothed using a Savitzky-Golay filter with a window size of 50 mm and channel thalwegs are identified with red circles. While all experiments experienced the same base-level rise rate, DB2-1701 shows a larger cross-section as it was allowed to aggrade for longer.

The DEM scans capture a snapshot of the delta topset only every hour, so we use the image data, which are much more frequent, to approximate some of this missing temporal information. Therefore, we developed a method for generating synthetic stratigraphy from overhead time-lapse photography. While images cannot provide elevation data, they give active channel locations throughout the experiment. All photos

were orthorectified and, using dyed water, we created binary maps of wet and dry regions based on an HSV color threshold (Wickert et al., 2013). Since the entire system experiences uniform base-level rise, the time step between images can be easily converted to a mean elevation change. Therefore, channels can be stacked in a way similar to the DEM process, except that the channel depth is not known.

To overcome this problem, we superimposed every DEM scan with the image corresponding to the nearest time step, allowing for depth measurements of active channels. For each of the three experiments, we measured channel width (B) and depth (h) from wet/dry images and DEM data, respectively. We then classified channels into width bins, (bin increment = 10 mm, and widths in the range $0<B<300$ mm). For each bin, we calculated an empirical distribution function of channel depth. This partition allows us to account for variation in channel aspect ratio ($\beta = B/h$) that emerges from our analyses (see Figs. A.2 and A.3). We then randomly selected a channel depth from the empirical distribution function associated with the local channel width, the latter being known from the wet/dry image. Using the same transect coordinates as the DEM data (Fig. 3.2A), we generated synthetic stratigraphy every 6 min from the images (Fig. 3.3) to allow for 9 additional horizons each hour as compared to the DEM data.

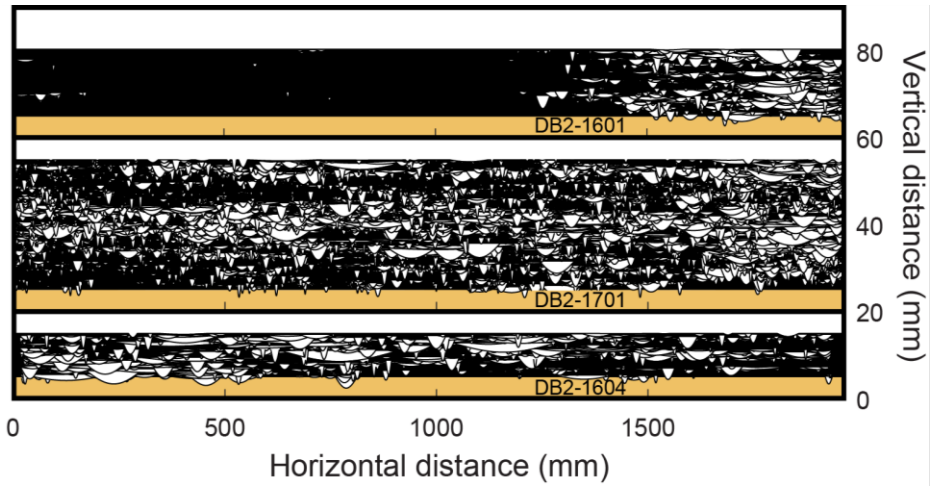

Figure 3.3: Image generated synthetic stratigraphy where each horizon depicts channel locations every 6 min. For every 10 mm of channel width, a bin was created of measured depths from DEM data. The sinuous depths depicted here were selected from a pdf based on the channel's width bin. Subsequent horizons clip lower elevations to represent areas of erosion.

RESULTS AND DISCUSSION

The synthetic stratigraphy results from both the DEM and image based methods show good correlation qualitatively (Figs. 3.2B and 3.3). This is encouraging as the DEM scans capture absolute topography and do not statistically assign channel depths. More importantly, both types of synthetic stratigraphy show a clear difference in distributary-channel body distribution from a system with strong tides (DB2-1601) to a system with no tides (DB2-1604). The stacking density of channel bodies has long been used as an index of channel mobility and avulsion rates both in the field (Allen, 1978; Bridge and Leeder, 1979; Mackey and Bridge, 1995; Mohrig et al., 2000), and in physical experiments (Sheets et al., 2007; Hajek et al., 2010). In the case of DB2-1601, the tides hold the main distributary channel captive in its location throughout the experiment. Small secondary channels periodically branch from the main channel to distribute sediment to other portions of the delta, but large areas are allowed to drown from the

overall base-level rise. This is not the case for DB2-1604, which had no tides yet the same values of sediment and water discharge. The distributary channels in this experiment effectively distribute sediment across the delta and maintain a relatively static shoreline (see Fig. A.4). Therefore, we expect systems with stronger tidal influence to display stratigraphy with higher channel connectivity and amalgamation due in part to decreased avulsion rates, and this is clearly visible in Figures 3.2B and 3.3.

Results for state change fraction per time (Fig. 3.1) show that even in a weakly tide-influenced delta (DB2-1701), the mobility of distributary channels is still reduced. In fact, both lateral migration and avulsion frequency drop significantly as tidal strength increases. The results for the synthetic stratigraphy for this case are not as clear; the channel bodies in DB2-1701 appear to show slightly higher stacking density than those found in the purely fluvial case (Figs. 3.2B and 3.3), the reduction in mobility is weaker and is not easily distinguished from the background noise. For a field comparison, a method such as the one developed by Hajek et al. (2010) to measure channel clustering may be useful in that tide-dominated deltas should display stronger grouping of channel bodies.

To compare our results to field cases, we must also consider the energy of the tidal and fluvial components of deltaic forcing. We use a method developed by Baumgardner (2015) to calculate energy-based tidal power and stress-based fluvial power metrics of a system. Tidal energy (Ω_T) is derived from the height of the tidal prism, H_T, and the tidal period, T, as

$$\Omega_T = \rho g H_T^3 / ST, \quad (1)$$

where ρ is the density of water, g is gravitational acceleration and S is the nearshore slope. Fluvial energy (Ω_F) is derived from channel discharge, Q, and slope, S, as

$$\Omega_F = \rho g Q S. \quad (2)$$

Both of these equations have units of W/m and represent the power per unit length in the streamwise direction (complete derivation is in Baumgardner, 2015). In our experiments the energy of the tides in DB2-1601 is higher than that of the fluvial power produced by the distributary-channels, while the opposite is true for DB2-1701 (Table 3.1). Comparing these energies with the mean state change fraction per time of the channels ($\overline{M}$), we see that, overall, the mobility of channels increases as relative tidal energy decreases (Fig. 3.4).

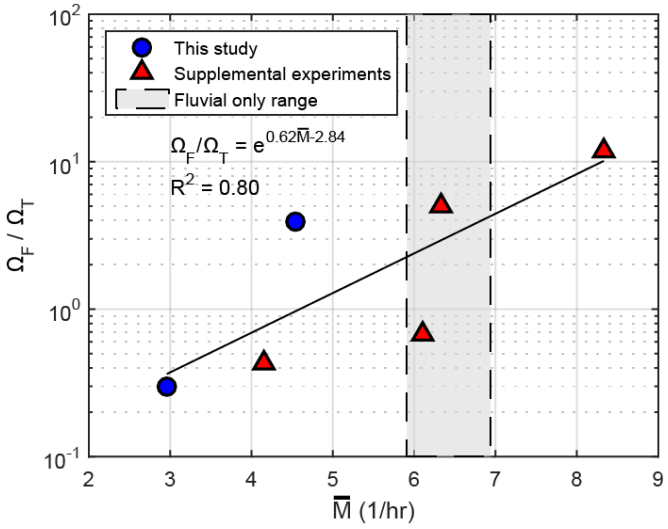

Figure 3.4: Relative fluvial (Ω_F) and tidal (Ω_T) energy versus the mean state change fraction per time ($\overline{M}$), here used as a proxy for mobility. This study consists of DB2-1601 and DB2-1701, while information on the supplemental experiments can be found in Table A.1 within the GSA Data Repository[1]. The fluvial only range represents the span of motilities found for experiments that had no tidal influence. Overall, as fluvial energy grows over tidal energy there is an increase in channel mobility.

We propose that the decrease in distributary-channel mobility, especially in terms of avulsion frequency, is due to the ability of tides to remobilize sediment distributed by the fluvial system. Tidal channels are formed and grow due to progressive erosion at their head, which is known from the field to occur mainly during the ebb phase (D'Alpaos et al., 2005). When a delta experiences base-level rise, as is the case for all experiments presented here, tidal inlets are forced to widen and deepen to accommodate the larger tidal prism (D'Alpaos et al., 2009). These effects together can remove large amounts of sediment that would otherwise be available to aggrade the beds of the channels. Whether one views superevelation (Heller and Paola, 1996) or critical levee slope (Mackey and Bridge, 1995) as the driver of channel avulsion, both mechanisms require deposition, a process that is impeded in the tidal deltas of this study. In the field, abundant fine sediment can in some cases allow net onshore tidal transport of sediment in off-channel areas, as for example in the Ganges-Brahmaputra-Meghna Delta of Bangladesh (Wilson and Goodbred, 2015). In that case, the channel-stabilization mechanism we describe here could be counteracted by the onshore fine-sediment transport.

Morphodynamic backwater effects can also drive deltaic channel mobility (Edmonds et al., 2009; Hoyal and Sheets, 2009). Edmonds et al. (2009) suggest that development of river mouth bars plays an important role in backwater avulsions. As the mouth bar reaches a critical size, it triggers a wave of bed aggradation that moves upstream, promoting overbank flows and levee erosion, eventually triggering an avulsion. Again, this mechanism requires deposition, especially near the shoreline, where in our experiments the influence of tidal erosion is greatest. We suggest that tides also act to

reduce avulsions by effectively removing this mouth-bar sediment. Overall, the two mechanisms we identify are both linked to the net removal of bed-material sediment from the channel network by tidal action.

[1]GSA Data Repository items can be found in Appendix A.

4

Conclusion

Within this thesis we have 1) used physical experiments to produce realistic tidal morphologies in a net depositional delta system, 2) developed methods for comparing shoreline position and transgression rates among datasets, as well as 3) established metrics to quantify net deposition on delta topsets, which together offer 4) a novel approach for tracking channel mobility in both fluvial- and tide-dominated environments, and finally with this approach 5) created synthetic stratigraphy from combined image and DEM data to link surface processes to the rock record. Combining these techniques and methods, our overall findings are that:

1. tide-influenced deltas show transgressive shorelines, regardless of tidal strength, under conditions in which fluvial deltas show shoreline stasis or regression;
2. the most dynamic fluvial-dominated delta system showed longitudinal profiles with up to two times the net deposition found in its tide-dominated and tide-influenced counterparts, pointing to sediment removal by tides;
3. as tide-influenced delta systems become more dynamic (i.e., high sediment discharge and high RSL rise rates), they transition from predominantly upstream deposition and downstream erosion to up- and downstream deposition;
4. strong tidal forcing can immobilize distributary channels and lead to composite

delta morphologies as tidal and fluvial processes dominate different regions of the delta;

5. tides act to reduce channel mobility, and mobility reduction increases as relative tidal strength increases;
7. the reduced mobility of distributary channels is reflected in stratigraphy as increased clustering and amalgamation of channel bodies;
6. synthetic stratigraphy created using images with statistical input from sparse DEM data shows good agreement to synthetic stratigraphy created from DEM data alone.

These experiments show the profound effect that tides have on distributary delta systems. Not only are they dominant in shaping the plan form morphology we see, but their influence on sediment transport can be found far offshore while their nearshore stabilization of channels will surely leave a signature in the rock record. As our understanding of tidal systems continues to evolve, we must consider how we identify tide-influenced deltas in the field, as well as how we model their response to continued sea-level rise.

A PATH FORWARD

After conducting numerous experiments with deltas affected by tidal forcing, it is clear that physical models are a viable tool for expanding our knowledge of depositional systems influenced by a range of allogenic forces. In fact, our original research goal was to include deltas affected by wave action as they represent a significant number of the world's deltas. DB-2 can produce depositional systems with wave forcing as the basin is

equipped with a wave generator. Using the methods we developed for tracking shoreline position, net deposition, channel mobility, and synthetic stratigraphy generation, future experiments with waves would greatly compliment the research presented here.

These experiments were partially inspired by the Venice Lagoon, a system with no fluvial input but strong tidal forcing and a chain of barrier islands which limits the inlets to the lagoon. It may be possible to use both tides and waves in conjunction to recreate a similar system and again test its response to sea-level rise, as this is of serious concern to everyone living on tidal deltas. Venice and its lagoon, for example, represent a world treasure under threat from rising sea level in conjunction with waves and tides. If anything, the research presented here has only inspired more work with several avenues of study branching from this initial tidal investigation.

Lastly, we hope for continued work on synthetic stratigraphy generators, especially in regards to teasing channel depths out of image data. The methods shown here still rely on DEM data and statistical analysis; however, it may be possible to limit the amount of DEM data needed and place more emphasis on the images themselves. Future work should focus on using a combination of active channel color from images and the color at control points where the depth is known. Ultimately, the fertility of such a tool would be great as it would drastically reduce costs for several types of research related to fluvial systems.

Like the tidal systems of this study, the ebb and flow of research is never truly done.

REFERENCES CITED

Ahnert, F., 1960, Estuarine meanders in the Chesapeake Bay Area: Geographical Review, v. 50, no. 3, p. 390–401, doi: 10.2307/212282.

Akter, J., Sarker, M., Popescu, I., and Roelvink, D., 2016, Evolution of the Bengal Delta: Journal of Coastal Research, v. 32, no. 5, p. 1212–1226.

Allen, J.R.L., 1978, Studies in fluviatile sedimentation: An exploratory quantitative model for the architecture of avulsion-controlled alluvial suites: Sedimentary Geology, v. 21, no. 2, p. 129–147, doi: 10.1016/0037-0738(78)90002-7.

Allison, M.A., 1998, Historical changes in the Ganges-Brahmaputra delta front: Journal of Coastal Research, v. 14, no. 4, p. 1269–1275.

Barrell, J., 1917, Rhythms and the measurements of geologic time: Geological Society of America Bulletin, v. 28, no. 1, p. 745–904, doi: 10.1130/GSAB-28-745.

Barua, D.K., 1990, Suspended sediment movement in the estuary of the Ganges-Brahmaputra-Meghna river system: Marine Geology, v. 91, no. 3, p. 243–253, doi: 10.1016/0025-3227(90)90039-M.

Barua, D.K., Kuehl, S.A., Miller, R.L., and Moore, W.S., 1994, Suspended sediment distribution and residual transport in the coastal ocean off the Ganges-Brahmaputra river mouth: Marine Geology, v. 120, p. 41–61, doi: 10.1016/0025-3227(94)90076-0.

Baumgardner, S.E., 2015, Quantifying Galloway: Fluvial, tidal and wave influence on experimental and field deltas [Ph.D. thesis]: University of Minnesota, 113 p.

Belknap, D.F., and Kraft, J.C., 1985, Influence of antecedent geology on stratigraphic

preservation potential and evolution of Delaware's barrier systems: Marine Geology, v. 63, no. 1–4, p. 235–262, doi: 10.1016/0025-3227(85)90085-4.

Bernier, N.B., and Thompson, K.R., 2010, Tide and surge energy budgets for Eastern Canadian and Northeast US waters: Continental Shelf Research, v. 30, no. 3–4, p. 353–364, doi: 10.1016/j.csr.2009.12.003.

Bhattacharya, J.P., and Giosan, L., 2003, Wave-influenced deltas: Geomorphological implications for facies reconstruction: Sedimentology, v. 50, no. 1, p. 187–210, doi: 10.1046/j.1365-3091.2003.00545.x.

Blum, M.D., and Törnqvist, T.E., 2000, Fluvial responses to climate and sea-level change: A review and look forward: Sedimentology, v. 47, p. 2–48, doi: 10.1046/j.1365-3091.2000.00008.x.

Boyd, R., Dalrymple, R., and Zaitlin, B.A., 1992, Classification of clastic coastal depositional environments: Sedimentary Geology, v. 80, no. 3–4, p. 139–150, doi: 10.1016/0037-0738(92)90037-R.

Bridge, J.S., and Jarvis, J., 1976, Flow and sedimentary processes in the meandering river South Esk, Glen Clova, Scotland: Earth Surface Processes, v. 1, no. 4, p. 303–336, doi: 10.1002/esp.3290010402.

Bridge, J.S., and Leeder, M.R., 1979, A simulation model of alluvial stratigraphy: Sedimentology, v. 26, no. 5, p. 617–644, doi: 10.1111/j.1365-3091.1979.tb00935.x.

Chen, Z., Song, B., Wang, Z., and Cai, Y., 2000, Late Quaternary evolution of the sub-aqueous Yangtze Delta, China: Sedimentation, stratigraphy, palynology, and deformation: Marine Geology, v. 162, no. 2–4, p. 423–441, doi: 10.1016/S0025-

3227(99)00064-X.

Church, J.A., Clark, P.U., Cazenave, A., Gregory, J.M., Jevrejeva, S., Levermann, A., Merrifield, M.A., Milne, G.A., Nerem, R.S., Nunn, P.D., Payne, A.J., Pfeffer, W.T., Stammer, D., and Unnikrishnan, A.S., 2013, Sea level change, *in* Stocker, T.F., Qin, D., Plattner, G.-K., Tignor, M., Allen, S.K., Boschung, J., Nauels, A., Xia, Y., Bex, V., and Midgley, P.M. eds., Climate Change 2013: The Physical Science Basis. Contribution of Working Group I to the Fifth Assessment Report of the Intergovernmental Panel on Climate Change, Cambridge University Press, Cambridge, p. 1137–1216.

D'Alpaos, A., Lanzoni, S., Marani, M., Fagherazzi, S., and Rinaldo, A., 2005, Tidal network ontogeny: Channel initiation and early development: Journal of Geophysical Research: Earth Surface, v. 110, no. 2, p. 1–14, doi: 10.1029/2004JF000182.

D'Alpaos, A., Lanzoni, S., Marani, M., and Rinaldo, A., 2009, On the O'Brien–Jarrett–Marchi law: Rendiconti Lincei, v. 20, no. 3, p. 225–236, doi: 10.1007/s12210-009-0052-x.

Dalrymple, R.W., and Choi, K., 2007, Morphologic and facies trends through the fluvial-marine transition in tide-dominated depositional systems: A schematic framework for environmental and sequence-stratigraphic interpretation: Earth-Science Reviews, v. 81, no. 3–4, p. 135–174, doi: 10.1016/j.earscirev.2006.10.002.

Edmonds, D.A., Hoyal, D.C.J.D., Sheets, B.A., and Slingerland, R.L., 2009, Predicting delta avulsions: Implications for coastal wetland restoration: Geology, v. 37, no. 8,

p. 759–762, doi: 10.1130/G25743A.1.

Ericson, J.P., Vörösmarty, C.J., Dingman, S.L., Ward, L.G., and Meybeck, M., 2006, Effective sea-level rise and deltas: Causes of change and human dimension implications: Global and Planetary Change, v. 50, no. 1–2, p. 63–82, doi: 10.1016/j.gloplacha.2005.07.004.

Ethridge, F.G., Germanoski, D., Schumm, S.A., and Wood, L.J., 2009, The morphological and stratigraphical effects of base-level change: A review of experimental studies, *in* Fluvial Sedimentology VII, Blackwell Publishing Ltd., p. 211–241.

Galloway, W.E., 1975, Process framework for describing the morphological and stratigraphic evolution of deltaic depositional systems, *in* Broussard, M.L. ed., Deltas: Models for Exploration, Houston Geological Society, Houston, p. 87–98.

Goodbred, S.L., and Kuehl, S.A., 1999, Holocene and modern sediment budgets for the Ganges-Brahmaputra river system: Evidence for highstand dispersal to flood-plain, shelf, and deep-sea depocenters: Geology, v. 27, no. 6, p. 559–562, doi: 10.1130/0091-7613(1999)027<0559:HAMSBF>2.3.CO;2.

Goodbred, S.L., and Saito, Y., 2012, Tide-dominated deltas, *in* Davis, R.A. and Dalrymple, R.W. eds., Principles of Tidal Sedimentology, Springer Science+Business Media B.V., p. 129–149.

Hajek, E.A., and Edmonds, D.A., 2014, Is river avulsion style controlled by floodplain morphodynamics? Geology, v. 42, no. 3, p. 199–202, doi: 10.1130/G35045.1.

Hajek, E.A., Heller, P.L., and Sheets, B.A., 2010, Significance of channel-belt clustering

in alluvial basins: Geology, v. 38, no. 6, p. 535–538, doi: 10.1130/G30783.1.

Hardisty, J., 2009, Modelling tidal stream power, *in* The Analysis of Tidal Stream Power, Wiley, West Sussex, p. 121–149.

Harris, P.T., Baker, E.K., Cole, A.R., and Short, S.A., 1993, A preliminary study of sedimentation in the tidally dominated Fly River Delta, Gulf of Papua: Continental Shelf Research, v. 13, no. 4, p. 441–472, doi: 10.1016/0278-4343(93)90060-B.

Heimann, D.C., Sprague, L.A., and Blevins, D.W., 2011, Trends in suspended-sediment loads and concentrations in the Mississippi River Basin, 1950–2009: U.S. Geological Survey Scientific Investigations Report 2011–5200, p. 33.

Heller, P.L., and Paola, C., 1996, Downstream changes in alluvial architecture; an exploration of controls on channel-stacking patterns: Journal of Sedimentary Research, v. 66, no. 2, p. 297–306, doi: 10.1306/D4268333-2B26-11D7-8648000102C1865D.

Hori, K., and Saito, Y., 2007, Classification, architecture, and evolution of large-river deltas, *in* Large Rivers, John Wiley & Sons, Ltd, p. 75–96.

Hoyal, D.C.J.D., and Sheets, B.A., 2009, Morphodynamic evolution of experimental cohesive deltas: Journal of Geophysical Research: Earth Surface, v. 114, no. 2, p. 1–18, doi: 10.1029/2007JF000882.

Hughes, Z.J., 2012, Tidal channels on tidal flats and marshes, *in* Davis, R.A. and Dalrymple, R.W. eds., Principles of Tidal Sedimentology, Springer Science+Business Media B.V., p. 269–300.

Kim, W., Paola, C., Voller, V.R., and Swenson, J.B., 2006, Experimental measurement of

the relative importance of controls on shoreline migration: Journal of Sedimentary Research, v. 76, no. 2, p. 270–283, doi: 10.2110/jsr.2006.019.

Kleinhans, M.G., Van Rosmalen, T.M., Roosendaal, C., and Van Der Vegt, M., 2014, Turning the tide: Mutually evasive ebb-and flood-dominant channels and bars in an experimental estuary: Advances in Geosciences, v. 39, p. 21–26, doi: 10.5194/adgeo-39-21-2014.

Kleinhans, M.G., Van Der Vegt, M., Terwisscha Van Scheltinga, R., Baar, A.W., and Markies, H., 2012, Turning the tide: Experimental creation of tidal channel networks and ebb deltas: Geologie en Mijnbouw/Netherlands Journal of Geosciences, v. 91, no. 3, p. 311–323, doi: 10.1017/S0016774600000469.

Kuehl, S.A., DeMaster, D.J., and Nittrouer, C.A., 1986, Nature of sediment accumulation on the Amazon continental shelf: Continental Shelf Research, v. 6, no. 1–2, p. 209–225, doi: 10.1016/0278-4343(86)90061-0.

Kuehl, S.A., Levy, B.M., Moore, W.S., and Allison, M.A., 1997, Subaqueous delta of the Ganges-Brahmaputra river system: Marine Geology, v. 144, no. 1–3, p. 81–96, doi: 10.1016/S0025-3227(97)00075-3.

Van De Lageweg, W.I., and Slangen, A.B.A., 2017, Predicting dynamic coastal delta change in response to sea-level rise: Journal of Marine Science and Engineering, v. 5, no. 2, p. 24, doi: 10.3390/jmse5020024.

Lanzoni, S., and D'Alpaos, A., 2015, On funneling of tidal channels: Journal of Geophysical Research: Earth Surface, v. 120, no. 3, p. 433–452, doi: 10.1002/2014JF003203.

Liu, J.P., Xue, Z., Ross, K., Wang, H.J., Yang, Z.S., Li, A.C., and Gao, S., 2009, Fate of sediments delivered to the sea by Asian large rivers: Long-distance transport and formation of remote alongshore clinothems: The Sedimentary Record, v. 7, no. 4, p. 4–9.

Mackey, S.D., and Bridge, J.S., 1995, Three-dimensional model of alluvial stratigraphy; theory and applications: Journal of Sedimentary Research, v. 65, no. 1b, p. 7–31.

Mahon, R.C., Shaw, J.B., Barnhart, K.R., Hobley, D.E.J., and Mcelroy, B., 2015, Quantifying the stratigraphic completeness of delta shoreline trajectories: Journal of Geophysical Research: Earth Surface, v. 120, p. 1–19, doi: 10.1002/2014JF003298.

Malverti, L., Lajeunesse, E., and Méttivier, F., 2008, Small is beautiful: Upscaling from microscale laminar to natural turbulent rivers: Journal of Geophysical Research: Earth Surface, v. 113, no. 4, p. 1–14, doi: 10.1029/2007JF000974.

Middleton, G.V., 1991, A short historical review of clastic tidal sedimentology, *in* Smith, D.G., Reinson, G.E., Zaitlin, B.A., and Rahmani, R.A. eds., Clastic Tidal Sedimentology, CSPG Special Publications, p. ix–xv.

Mohrig, D., Heller, P.L., and Lyons, W.J., 2000, Interpreting avulsion process from ancient alluvial sequences: Guadalope-Matarranya system (northern Spain) and Wasatch Formation (western Colorado): Geological Soceity of America Bulletin, v. 112, no. 12, p. 1787–1803, doi: 10.1130/0016-7606(2000)112<1787:IAPFAA>2.0.CO;2.

Nienhuis, J.H., Ashton, A.D., and Giosan, L., 2015, What makes a delta wave-dominated? Geology, v. 43, no. 6, p. 511–514, doi: 10.1130/G36518.1.

Nittrouer, C.A., Kuehl, S.A., Demaster, D.J., and Kowsmann, R.O., 1986, The deltaic nature of Amazon shelf sedimentation: Geological Society of America Bulletin, v. 97, no. 4, p. 444–458, doi: 10.1130/0016-7606(1986)97<444:TDNOAS>2.0.CO;2.

Paola, C., Straub, K., Mohrig, D., and Reinhardt, L., 2009, The "unreasonable effectiveness" of stratigraphic and geomorphic experiments: Earth-Science Reviews, v. 97, no. 1–4, p. 1–43, doi: 10.1016/j.earscirev.2009.05.003.

Pizzuto, J.E., 1987, Sediment diffusion during overbank flows: Sedimentology, v. 34, no. 2, p. 301–317, doi: 10.1111/j.1365-3091.1987.tb00779.x.

Plink-Björklund, P., 2012, Effects of tides on deltaic deposition: Causes and responses: Sedimentary Geology, v. 279, p. 107–133, doi: 10.1016/j.sedgeo.2011.07.006.

Sadler, P.M., 1981, Sediment accumulation rates and the completeness of stratigraphic sections: The Journal of Geology, v. 89, no. 5, p. 569–584, doi: 10.1086/628623.

Schafer, R.W., 2011, What is a savitzky-golay filter? IEEE Signal Processing Magazine, v. 28, no. 4, p. 111–117, doi: 10.1109/MSP.2011.941097.

Sheets, B.A., Paola, C., and Kelberer, J.M., 2007, Creation and preservation of channel-form sand bodies in an experimental alluvial system, *in* Nichols, G., Williams, E., and Paola, C. eds., Sedimentary processes, environments and basins, Oxford, Blackwell, p. 555–567.

Slingerland, R., Driscoll, N.W., Milliman, J.D., Miller, S.R., and Johnstone, E.A., 2008, Anatomy and growth of a Holocene clinothem in the Gulf of Papua: Journal of Geophysical Research: Earth Surface, v. 113, no. 1, p. 1–16, doi: 10.1029/2006JF000628.

Slingerland, R., and Smith, N.D., 1998, Necessary conditions for a meandering-river avulsion: Geology, v. 26, no. 5, p. 435–438, doi: 10.1130/0091-7613(1998)026<0435:NCFAMR>2.3.CO.

Stefanon, L., Carniello, L., D'Alpaos, A., and Lanzoni, S., 2010, Experimental analysis of tidal network growth and development: Continental Shelf Research, v. 30, no. 8, p. 950–962, doi: 10.1016/j.csr.2009.08.018.

Strahler, A.N., 1957, Quantitative analysis of watershed geomorphology: Eos, Transactions American Geophysical Union, v. 38, no. 6, p. 913–920, doi: 10.1029/TR038i006p00913.

Swanson, K.M., Watson, E., Aalto, R., Lauer, J.W., Bera, M.T., Marshall, A., Taylor, M.P., Apte, S.C., and Dietrich, W.E., 2008, Sediment load and floodplain deposition rates: Comparison of the Fly and Strickland rivers, Papua New Guinea: Journal of Geophysical Research: Earth Surface, v. 113, no. 1, p. 2–17, doi: 10.1029/2006JF000623.

Swenson, J.B., 2005, Relative importance of fluvial input and wave energy in controlling the timescale for distributary-channel avulsion: Geophysical Research Letters, v. 32, no. 23, p. 1–5, doi: 10.1029/2005GL024758.

Swenson, J.B., Paola, C., Pratson, L., Voller, V.R., and Murray, A.B., 2005, Fluvial and marine controls on combined subaerial and subaqueous delta progradation: Morphodynamic modeling of compound-clinoform development: Journal of Geophysical Research: Earth Surface, v. 110, no. 2, p. 1–16, doi: 10.1029/2004JF000265.

Swenson, J.B., Voller, V.R., Paola, C., Parker, G., and Marr, J.G., 2000, Fluvio-deltaic sedimentation: A generalized Stefan problem: European Journal of Applied Mathematics, v. 11, no. 5, p. 433–452.

Tambroni, N., Bolla Pittaluga, M., and Seminara, G., 2005, Laboratory observations of the morphodynamic evolution of tidal channels and tidal inlets: Journal of Geophysical Research: Earth Surface, v. 110, no. 4, doi: 10.1029/2004JF000243.

Tänavsuu-Milkeviciene, K., and Plink-Björklund, P., 2009, Recognizing tide-dominated versus tide-influenced deltas: Middle Devonian strata of the Baltic Basin: Journal of Sedimentary Research, v. 79, no. 12, p. 887–905, doi: 10.2110/jsr.2009.096.

Tejedor, A., Longjas, A., Zaliapin, I., and Foufoula-Georgiou, E., 2015, Delta channel networks: 2. Metrics of topologic and dynamic complexity for delta comparison, physical inference, and vulnerability assessment: Water Resources Research, v. 51, no. 6, p. 4019–4045, doi: 10.1002/2014WR016604.

Tian, G., Jiang, J., Yang, Z., and Zhang, Y., 2011, The urban growth, size distribution and spatio-temporal dynamic pattern of the Yangtze River Delta megalopolitan region, China: Ecological Modelling, v. 222, no. 3, p. 865–878, doi: 10.1016/j.ecolmodel.2010.09.036.

Vlaswinkel, B.M., and Cantelli, A., 2011, Geometric characteristics and evolution of a tidal channel network in experimental setting: Earth Surface Processes and Landforms, v. 36, no. 6, p. 739–752, doi: 10.1002/esp.2099.

Wickert, A.D., Martin, J.M., Tal, M., Kim, W., Sheets, B., and Paola, C., 2013, River channel lateral mobility: Metrics, time scales, and controls: Journal of Geophysical

Research: Earth Surface, v. 118, no. 2, p. 396–412, doi: 10.1029/2012JF002386.

Wilson, C.A., and Goodbred, S.L., 2015, Construction and maintenance of the Ganges-Brahmaputra-Meghna Delta: Linking process, morphology, and stratigraphy: Annual Review of Marine Science, v. 7, no. 1, p. 67–88, doi: 10.1146/annurev-marine-010213-135032.

Woodroffe, C.D., Nicholls, R.J., Saito, Y., Chen, Z., and Goodbred, S.L., 2006, Landscape variability and the response of asian megadeltas to environmental change, *in* Harvey, N. ed., Global Change and Integrated Coastal Management, Springer Netherlands, Dordrecht, p. 277–314.

Wright, L.D., Coleman, J.M., and Thom, B.G., 1973, Processes of channel development in a high-tide-range environment: Cambridge Gulf-Ord River Delta, Western Australia: The Journal of Geology, v. 81, no. 1, p. 15–41.

A

Appendix A: GSA Data Repository

EXPERIMENTAL METHODS

All experiments (Table A.1) were conducted at Saint Anthony Falls Laboratory in the Delta Basin-2 (DB-2) facility. This basin has the capability of producing deltaic deposits subjected to tidal forcing (Fig. A.1). The main basin is square, 5 m by 5 m, and has a depth of 0.5 m. The northwest corner of the basin is fed well-mixed sediment and water, which is precisely computer controlled, to create a semicircular delta lobe. The point source of sediment and water is located behind a rock wall which acts as a diffuser to help minimize local turbulence and scour. Base level is also computer controlled by utilizing a motorized weir which is in sync with an ocean elevation sensor that takes water depth measurements every 5 seconds. There is not a direct method of creating subsidence as the bottom of the basin is static, however raising base level can be thought of as either sea-level rise or comparatively as subsidence.

TABLE A.1 EXPERIMENT PARAMETERS AND ENERGIES

Experimen	Sea-level Rise (mm/hr)	Water Discharge (m^3/s)	Sediment Discharge (m^3/s)	Tide Amplitude (mm)	Tide Period (sec)	Tidal Power (W/m)*	Fluvial Power (W/m)*	Total Aggradatio (mm)
DB2-1601	**0.5**	**5.0e-5**	**5.0e-7**	**10.0**	**120**	**3.27e-2**	**9.81e-3**	**10.0**
DB2-1701	**0.5**	**5.0e-5**	**5.0e-7**	**3.5**	**120**	**1.87e-3**	**7.36e-3**	**30.0**
DB2-1604	**0.5**	**5.0e-5**	**5.0e-7**	**N/A†**	**N/A†**	**N/A†**	**7.85e-3**	**10.0**
DB2-1607	1.0	1.0e-4	1.0e-6	10.0	120	3.85e-2	1.67e-2	28.0
DB2-1608	1.0	1.0e-4	1.0e-6	3.5	120	2.34e-3	1.18e-2	29.0
DB2-1605	1.0	1.0e-4	1.0e-6	N/A†	N/A†	N/A†	1.37e-2	30.0
DB2-1606	2.0	2.0e-4	2.0e-6	10.0	120	4.36e-2	2.94e-2	30.0
DB2-1603	2.0	2.0e-4	2.0e-6	3.5	120	2.16e-3	2.55e-2	98.0
DB2-1602	2.0	2.0e-4	2.0e-6	N/A†	N/A†	N/A†	2.55e-2	100.0

Note: The bold experiments were the focus of the article while the supplemental experiments were used in Figure 3.4.

*Calculated with the energy-based tidal power metrics and stress-based fluvial power metrics of Baumgardner (2015).

†N/A = not applicable; these experiments did not include tides.

To create tides, water is transferred by two industrial pumps from the main basin to a connected auxiliary basin. This 2 m by 2 m basin has a similar depth of 0.5 m and stores the volume of water necessary to create a desired tidal range in the main basin. During the flood phase of the tidal cycle, water is pumped into the main basin by the flood pump. After the specified upper tidal limit is reached, the flood pump ceases allowing for a slack water condition on the delta. The ebb pump then brings the water level down to the lower tidal limit and again allows for a momentary slack water condition. The tidal amplitude, or half the tidal range, and the tidal period are both user defined in a computer control system. The tidal cycle for these experiments is perfectly sinusoidal and any deviations from the specified water elevation are identified by the difference in measured water depth and computer calculated water depth. Small changes in voltage to the pumps and elevation to the weir produce an error of less than 1 mm in water elevation. It is important to note that the current programing in DB-2 does not allow for mixed tidal ranges. In nature, several tide-influenced systems experience mixed

semidiurnal tide cycles, i.e. they have two high tides and two low tides of different magnitude. However, most of the world's coastlines experience diurnal and semidiurnal tidal cycles (Hardisty, 2009), and are thus represented well by these experiments.

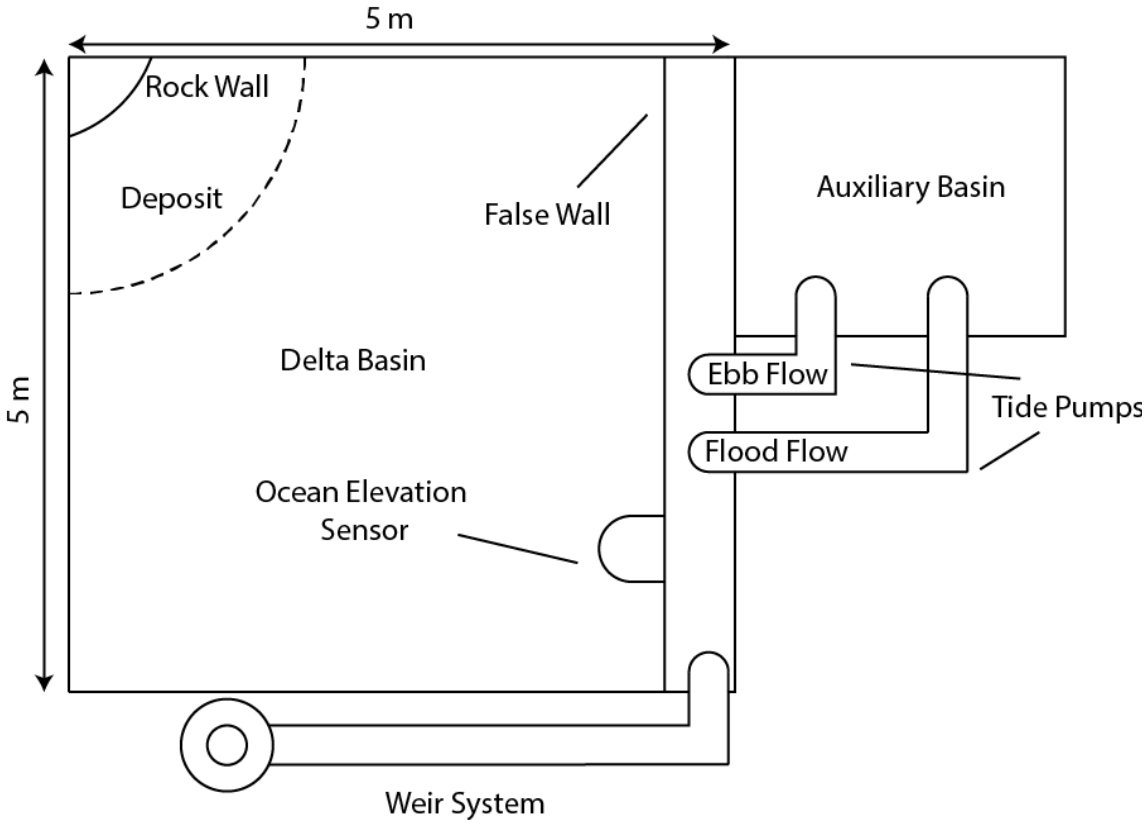

Figure A.1: Schematic of Delta Basin-2 from Baumgardner (2015). The weir system works in conjunction with the ocean elevation sensor to maintain the desired ocean level. The tide pumps bring water in and out of the basin from an auxiliary basin to create the tides. The inlets of the pumps are behind a false wall in the main basin to minimize any currents created by the point sources (i.e., the flood and ebb pipes).

IMAGE BASED CHANNEL DEPTH STATISTICS

For purposes of statistically assigning channel depths to channels identified in images, we superimposed every DEM scan with the image corresponding to the nearest time step, allowing for depth measurements of active channels. For each of the three experiments, channel width (B) and depth (h) measurements are therefore derived from

wet/dry images and DEM data, respectively. Channels are then classified into different bins, according to their width (each bin size corresponds to 10 mm, and the analyses span the range $0<B<300$ mm). Within every bin, we calculate the empirical distribution function of channel depth. This partition allows us to account for the nonlinearity in channel aspect ratio ($\beta = B/h$) that emerges from our analyses (see Fig. A.2). We then randomly select a channel depth (h_0^*) from the empirical distribution function associated with the local channel width (B_0^*), the latter being known from the wet/dry image.

When a channel maintains its position over two consecutive time-steps, giving rise to a stacked-channel pattern, we assign the uppermost channel a depth value of h_1^*-selected from the probability distribution corresponding to the width B_1^* of the considered channel - whose experimental probability $p(h_1^*)$ equals $p(h_0^*)$, where $p(h_0^*)$ is conditional to B_0^* of the lower stacked channel. This is provided that two stacked channels are considered related to each other only if the relative variation of their width does not exceed 25% ($|B_0^*/B_1^*|<0.25$), this assumption is demonstrated to be applicable as the variations of depth ($\Delta h^*=h_0^*-h^*$) for stacked channels are negligible over the entire variability range of channel width (see Fig. A.3).

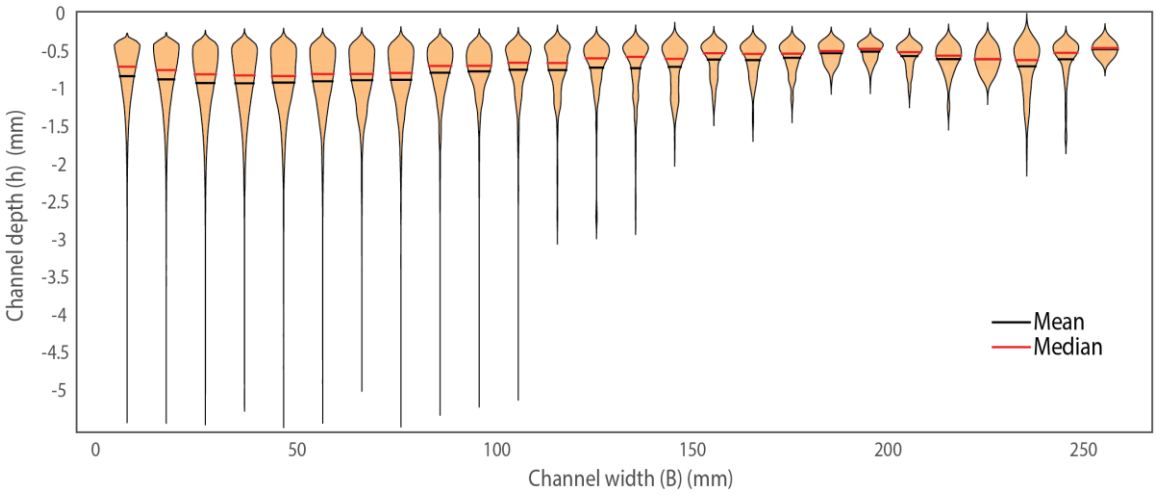

Figure A.2: Violin plot of channel depth (*h*) binned according to the corresponding channel width (*B*) for experiment DB2-1701. The mean (black lines) and the median (red lines) of the distributions are also shown.

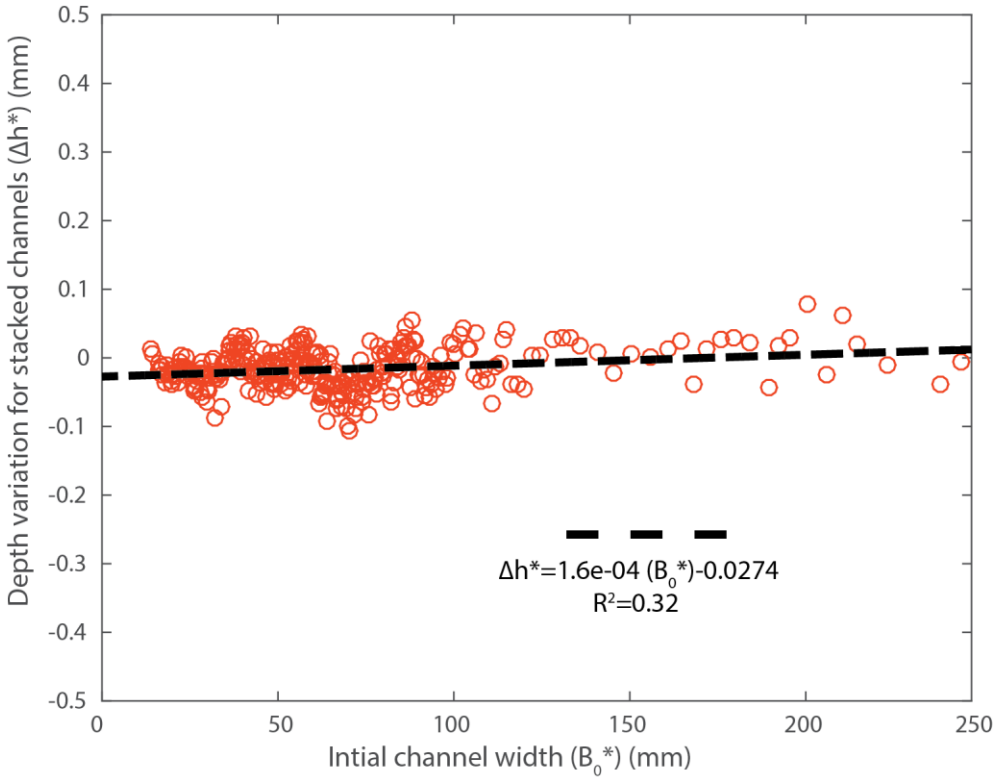

Figure A.3: Variation of depth for stacked channels (Δh^*) is plotted against width of the lowermost stacked channel (B_0^*) for experiment DB2-1701. The dotted line represents the best linear fit for the observed data.

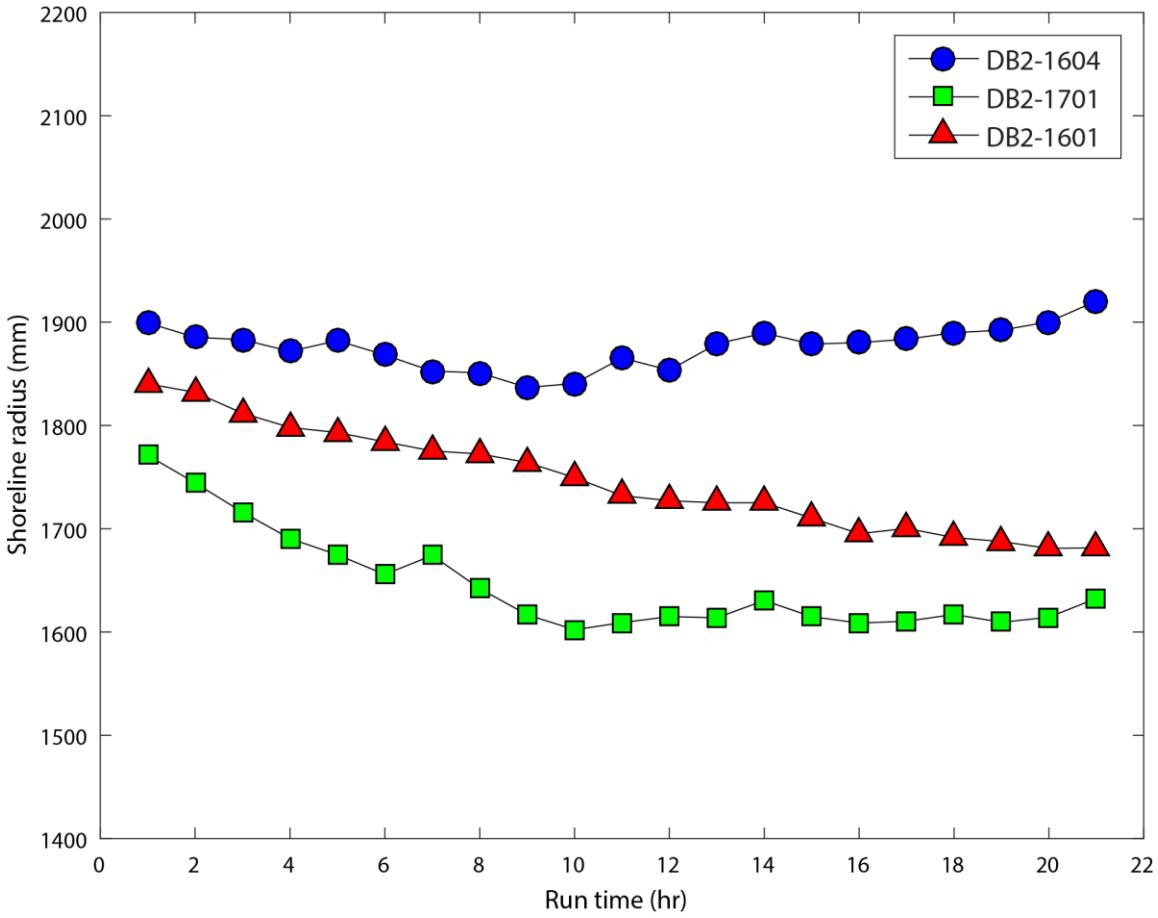

Figure A.4: Mean shoreline position thru time. The fluvial only experiment (DB2-1604) shows a static shoreline radius, while both 10 mm tides (DB2-1601) and 3.5 mm tides (DB2-1701) experiments show transgression.

REFERENCES CITED

Baumgardner, S.E., 2015, Quantifying Galloway: Fluvial, tidal and wave influence on experimental and field deltas [Ph.D. thesis]: University of Minnesota, 113 p.

Hardisty, J., 2009, Modelling tidal stream power, *in* The Analysis of Tidal Stream Power, Wiley, West Sussex, p. 121–149.